



Iridium complexes of acridine-based PNP-type pincer ligands: Synthesis, structure and reactivity

Yarden Lavi^a, Michael Montag^{a,*}, Yael Diskin-Posner^b, Liat Avram^b, Linda J.W. Shimon^b, Yehoshua Ben-David^a, David Milstein^{a,*}

^a Department of Molecular Chemistry and Materials Science, Weizmann Institute of Science, Rehovot, Israel

^b Department of Chemical Research Support, Weizmann Institute of Science, Rehovot, Israel



ARTICLE INFO

Keywords:
Iridium complex
PNP pincer
AcrPNP
Oxidative addition
H₂ addition
C—H activation

ABSTRACT

Acridine-based PNP-type pincer ligands (AcrPNP) have previously been used for the construction of a small number of Ru(II), Mn(I), Rh(III) and Ir(III) complexes, with most attention being given to the catalytically-active ruthenium complexes. In the present work, we significantly expand the scope of known AcrPNP complexes by introducing a series of new Ir(I) and Ir(III) complexes. These were synthesized from two AcrPNP ligands differing in their P-substituents (¹Pr vs Ph), in conjunction with various Ir(I)-olefin precursors, through different sequences of reactions that include intramolecular C—H activations and additions of H₂ and NaBET₃H. The new iridium complexes, with their observed structures and reactivities, reflect the unique properties of the acridine-based PNP ligands, i.e., their inherent structural flexibility and ability to support both metal-centered reactivity (C—H and H—H oxidative addition) and ligand-centered reactivity (hydride- and H₂-induced dearomatization).

1. Introduction

Acridine-based PNP-type pincer ligands of the general form 4,5-bis(dialkylphosphinomethyl)acridine (AcrPNP; Fig. 1) were introduced by our group over a decade ago [1], and have since been used primarily for the development of homogenous ruthenium-based catalytic systems that promote a variety of sustainable organic transformations [2]. The structures of the corresponding precatalysts and catalysts explored by us [1,3–9], and by others [10–12], are depicted in Scheme 1. A notable characteristic of the AcrPNP ligands, which sets them apart from the more commonly-used pyridine-derived PNP ligands, is the electrophilicity of the acridine C9 position [2]. This allows one to dearomatize the central ring of the acridine fragment in a given complex of AcrPNP by simply adding an appropriate nucleophile. The aforementioned precatalysts were converted into active catalysts through such dearomatizations, using various hydride donors (Scheme 1), namely, H₂, alcohol or amine via base-assisted reactions [4,10,13–15], or, more recently, triethylborohydride [9]. It should be noted that this type of dearomatization is fundamentally different from the well-documented deprotonation-induced dearomatization of pyridine-based PNP- and PNN-type pincer complexes, which is usually reversible and underlies their unique bond-activation capabilities (Scheme 2) [16]. By contrast, the

dearomatization of AcrPNP complexes appears to be irreversible, at least in the case of ruthenium complexes, which were the focus of most previous studies involving these ligands [2]. Nevertheless, in both the acridine- and pyridine-based systems, dearomatization is a prerequisite for precatalyst activation.

Another noteworthy property of the acridine-derived PNP ligands is that they are more flexible than the pyridine-based ones. They generate six- rather than five-membered metallacycles upon coordination, and their two chelating side-arms are capable of both *trans*- and *cis*-coordination, as has been documented [4,8,10,17]. This flexibility is most pronounced in complexes involving the dearomatized variants of the AcrPNP ligands, since the reduced acridanide (9*H*-acridinide) moiety is more pliable than the parent acridine. We have shown that in ruthenium complexes, such dearomatized AcrPNP ligands can interconvert between meridional and facial coordination geometries with relative ease [5–7], thereby enabling unique catalytic activity [8,9,18–20].

While the chemistry of AcrPNP-Ru complexes has been explored quite extensively, particularly in the context of catalysis, little attention has been devoted to complexes of other metals. Thus, the synthesis and characterization of a few manganese complexes was recently reported by us [21], and two group 9 complexes, one containing rhodium and the other iridium, have appeared in a patent by Zuo involving catalytic

* Corresponding authors.

E-mail addresses: michael.montag@alumni.weizmann.ac.il (M. Montag), david.milstein@weizmann.ac.il (D. Milstein).

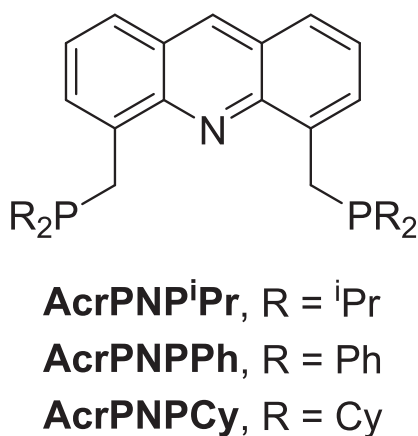


Fig. 1. Representative examples of acridine-based PNP-type (AcrPNP) pincer ligands.

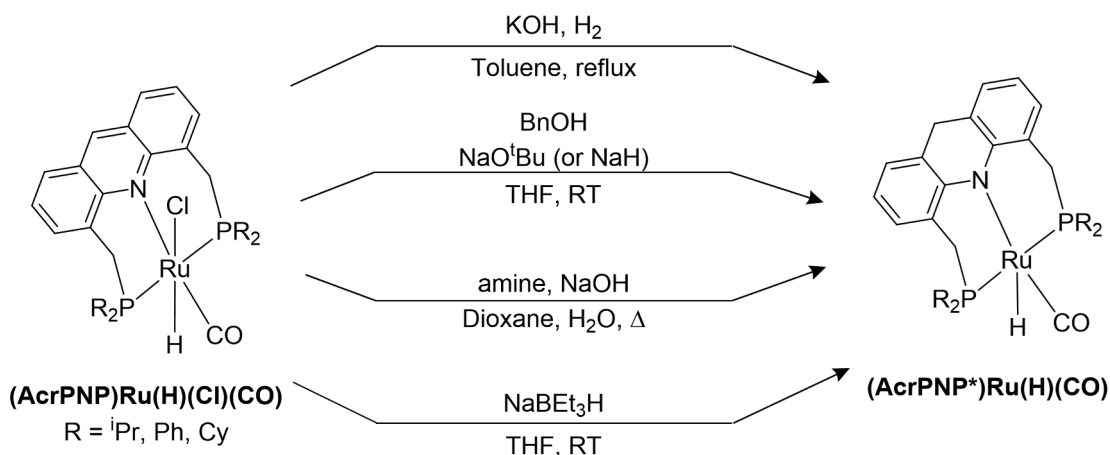
alcohol amination [22]. A catalytic hydrogenation system involving an Ir(I) precursor and an AcrPNP ligand has been examined by Zhou and coworkers, but the resulting complex was not characterized [23]. As part of our own efforts to develop catalysts for various reactions involving C—H activation, we sought to investigate AcrPNP-iridium complexes as potential candidates. In the present report, we describe a series of new neutral, cationic and anionic iridium complexes featuring ⁱPr- and Ph-substituted AcrPNP ligands, as well as their acridanide variants. These complexes were obtained through various sequences of reactions, including intramolecular C—H activations and additions of H₂ and NaBEt₃H, and they reflect the unique properties of the acridine-based PNP ligands, i.e., their ability to undergo facile dearomatization and inherent structural flexibility.

2. Results and discussion

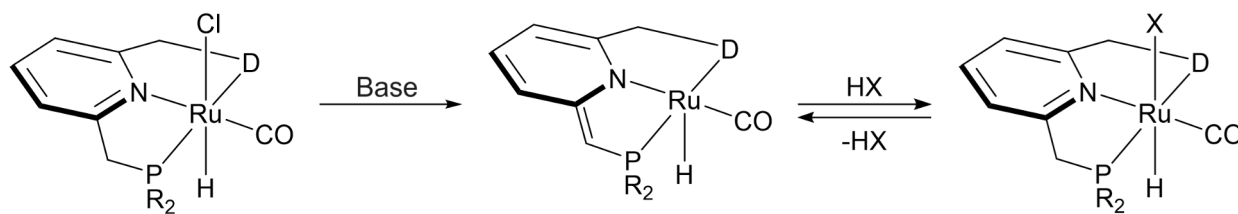
Our work on AcrPNP-Ir complexes involved two pincer ligands, namely, the ⁱPr-substituted AcrPNPⁱPr and the Ph-substituted AcrPNPPh (Fig. 1). Initially, each of these ligands was allowed to react in THF, at room temperature, with 0.5 equiv of the dimeric Ir(I) precursor [Ir(ethylene)₂Cl]₂, prepared *in situ* from the parent dimer [Ir(COE)₂Cl]₂ (COE = η^2 -cyclooctene) and excess ethylene gas. In the case of AcrPNPⁱPr, the reaction afforded the Ir(III) complex **1** (Scheme 3), which was isolated in high yield, typically around 90%. This asymmetric complex, featuring a cyclometalated pincer side-arm and an ethyl ligand, gives

rise to two doublets in its ³¹P{¹H} NMR spectrum in THF-d₈, at 10.2 and -30.0 ppm, with a 1:1 integral ratio. The two-bond ³¹P-³¹P coupling constant for these nuclei (²J_{PP}) is relatively small, at 19.5 Hz, and is consistent with a *cis* configuration of the two phosphine donors [24], indicating that this AcrPNP ligand is facially coordinated to the metal center. In the ¹H NMR spectrum, the pincer side-arms are represented by two distinct resonances with a 2:1 integral ratio, namely, a multiplet at 3.76 ppm corresponding to the methylene moiety of the intact side-arm, and a doublet-of-doublets at 3.05 ppm (²J_{PH} = 5.0 Hz, ³J_{PH} = 2.3 Hz) that is assigned to the methine group of the cyclometalated side-arm. The ethyl ligand gives rise to two multiplets, at 2.23 and 0.94 ppm, attributed to its CH₂ and CH₃ groups, respectively. In the ¹³C{¹H} NMR spectrum, the CH₂ moiety of this ethyl ligand resonates at -22.9 ppm. Full characterization details for this complex, as well as all other new complexes discussed in this report, are provided in the Experimental Section and *Supplementary Information*. It is likely that complex **1** is generated through intramolecular C—H oxidative addition at the benzylic position of one of the pincer side-arms upon coordination of AcrPNPⁱPr to the Ir(I) precursor, followed by migratory insertion of the resulting hydride into an ethylene ligand carried over from that precursor, resulting in the observed ethyl ligand. Similar side-arm activation has been reported previously for a ruthenium complex of a cyclohexyl-substituted AcrPNP ligand [10].

Interestingly, when AcrPNPⁱPr was replaced by AcrPNPPh, reaction with 0.5 equiv of [Ir(ethylene)₂Cl]₂ in THF did not simply result in a Ph-substituted analog of **1**, but instead generated the noncyclometalated Ir(I) complex **2**, bearing an ethylene ligand. This complex, which was isolated in nearly quantitative yield, proved to be practically insoluble in most conventional solvents, but is soluble in dichloromethane. However, it was found to be unstable in CD₂Cl₂ at room temperature, and therefore its NMR analysis was performed at -10 °C. Under these conditions, its ³¹P{¹H} NMR spectrum displays two doublets, at 24.6 and 11.5 ppm, with a 1:1 integral ratio, in line with an asymmetric structure, and a relatively small ²J_{PP} value of 17.4 Hz, which is consistent with a *cis* configuration of the two phosphine donors. In the ¹H NMR spectrum, the ethylene ligand gives rise to four multiplets between 2.50 and -0.05 ppm, and its ¹³C{¹H} NMR resonances appear as a doublet at 26.9 ppm (²J_{CP} = 41.0 Hz) and a singlet at 26.3 ppm. Thus, all atoms comprising ethylene are chemically inequivalent, clearly showing that this ligand is locked in position at -10 °C, and does not freely rotate about the Ir—ethylene axis on the NMR timescale. Moreover, all of these NMR peaks are shifted significantly upfield relative to solvated ethylene, for which δ(¹H) = 5.40 ppm and δ(¹³C) = 123.2 ppm in CD₂Cl₂ at room temperature [25], thereby indicating the existence of strong Ir → C=C back-donation in the ethylene complex, as also suggested by the C—C bond length of the coordinated ethylene (see below). Similar upfield shifts of



Scheme 1. The previously reported ruthenium precatalysts (AcrPNP)Ru(H)(Cl)(CO) and corresponding dearomatized catalysts (AcrPNP*)Ru(H)(CO) generated through reaction of the former with various hydride sources. RT, room temperature.



Scheme 2. Reversible dearomatization of pyridine-based PNP- and PNN-type pincer ligands in representative Ru complexes, and related bond activation reactions. D = PR₂, NR₂ (R = alkyl, aryl). HX = H₂, H₂O, ROH, RNH₂, etc. Such reactivity was also observed for similar complexes of other transition metals (e.g., Rh, Ir, Re, Fe).

ethylene ¹H and ¹³C NMR resonances were previously observed for the structurally-related complex *trans*-Ir[PH(¹Bu)₂]₂(Cl)(ethylene) [26]. However, in contrast to the latter, the ethylene ligand in complex **2** is positioned *trans* to one of the P-donors, as indicated by the multiplicity of one of the ¹³C{¹H} NMR signals associated with this ethylene moiety - a doublet with a relatively large two-bond ³¹P-¹³C coupling constant (41.0 Hz) - and as clearly demonstrated by the crystal structure of this complex.

The molecular structure of **2** was confirmed by X-ray crystallographic analysis of an appropriate crystal grown at ambient temperature from a dichloromethane solution overlaid with pentane. The complex crystallized in the monoclinic space group *P2*₁/*n*, and its solid-state structure is shown in Fig. 2 (crystallographic data for all crystal structures discussed in this work are provided in Table S1 of the Supplementary Information). As would be expected of an Ir(I) complex, **2** displays a formally square-planar coordination geometry defined by two *cis*-chelating phosphine donors, a chloride and an ethylene ligand positioned perpendicular to the plane containing the IrP₂Cl fragment. It is noteworthy that the carbon–carbon bond of the coordinated ethylene in **2**, measuring 1.425(6) Å, is substantially longer than the average of 1.38(1) Å calculated for the respective bonds in the three structurally-related *cis*-Ir(PR₃)₂(Cl)(ethylene) complexes found in the Cambridge Structural Database (CSD; v. 5.43) [26–28]. In fact, the length of the ethylene carbon–carbon bond in **2** is essentially halfway between free ethylene [1.339(1) Å] [29] and ethane [1.534(2) Å] [30]. These data, together with the NMR findings, indicate that complex **2** exhibits strong Ir → C=C backdonation, significantly reducing the carbon–carbon bond order and leading to its marked elongation. It should also be noted that the Ir–N distance, at 2.749(3) Å, is over 30% shorter than the sum of van der Waals (vdW) radii of the respective atoms ($r_{\text{Ir}} + r_{\text{N}} = 2.41 \text{ \AA} + 1.66 \text{ \AA} = 4.07 \text{ \AA}$) [31], suggesting the existence of some interaction between the metal center and acridine N-donor, although the extent of bonding is unclear. It may be that the ethylene ligand, being a strong π-acceptor, lowers the electron density at the metal center, thereby promoting its interaction with the neighboring nitrogen donor.

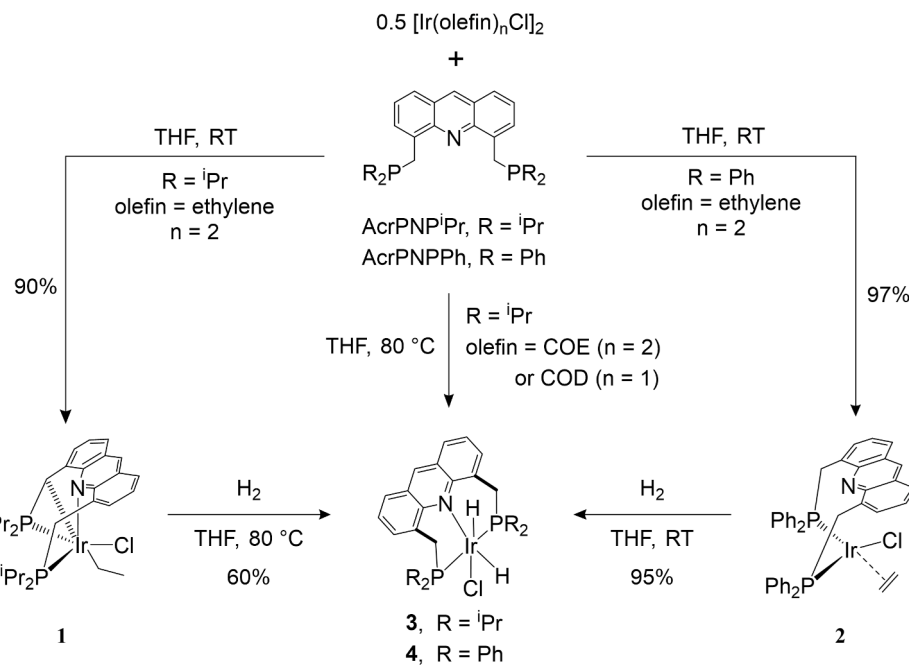
The fact that [Ir(ethylene)₂Cl]₂ reacts with AcrPNPⁱPr to give a cyclometalated Ir(III) product (**1**), whereas its reaction with AcrPNPPh affords a noncyclometalated Ir(I) product (**2**), attests to the different electronic properties of the P-donors of the two pincer ligands. The ⁱPr-substituted phosphines of AcrPNPⁱPr are stronger electron donors and weaker acceptors than the Ph-substituted phosphines of AcrPNPPh, and therefore the former pincer ligand renders the iridium center more “electron-rich” and hence more prone to C–H oxidative addition. Nevertheless, despite the divergent effects of their pincer ligands, both complexes **1** and **2** were found to be reactive enough to oxidatively add H₂. Thus, treating each of these complexes with excess dihydrogen (2 bar) in THF afforded the respective dihydrido complexes, **3** and **4** (Scheme 3), which are structurally analogous to each other. Complex **2** emerged as much more reactive than **1**, with the former being fully

consumed within 1 h at room temperature under 2 bar of H₂, whereas the latter required heating at a nominal temperature[†] of 80 °C to reach full conversion under otherwise identical conditions. We were able to isolate the resulting complex **3** in fair yield, typically around 60%, whereas **4** could be isolated in nearly quantitative yield. It should be noted that the divergent reactivity of complexes **1** and **2** vis-à-vis H₂ oxidative addition can be clearly attributed to their distinct structural and electronic properties. Thus, **2** is a square-planar d⁸ Ir(I) species that can directly and readily react with H₂ [32–34], whereas **1** is an octahedral d⁶ Ir(III) species that requires prior activation, most likely through conversion into a square-planar d⁸ species analogous to **2**. This can be accomplished, for example, through β-hydride elimination of the ethyl ligand of **1**, followed by C–H reductive elimination to release the pincer side-arm.

The ³¹P{¹H} NMR spectrum of complex **3** in C₆D₆ displays a sharp singlet at 55.5 ppm, clearly indicating that the two phosphine donors are chemically equivalent, in line with the C_s symmetry of the proposed structure, having a mirror plane that contains the IrH₂Cl fragment and bisects the acridine scaffold. Its ¹H NMR spectrum features two triplet-of-doublets signals at -23.21 ppm (²J_{PH} = 18.1 Hz, ²J_{HH} = 7.8 Hz) and -28.64 ppm (²J_{PH} = 15.7 Hz, ²J_{HH} = 7.9 Hz), associated with two distinct hydride ligands, and their relatively small coupling constants indicate that these hydrides are *cis* to each other, as well as to both phosphine donors [35]. Combined together, these NMR data are consistent with meridional coordination of the AcrPNPⁱPr pincer ligand in complex **3**, and its overall structure as shown in Scheme 3. This was further corroborated by the crystal structure of this complex, which is depicted in Fig. 3, and is based on X-ray diffraction data from a crystal grown at room temperature from a THF solution of the complex overlaid with pentane. The complex, which co-crystallized with an adventitious water molecule in the trigonal space group R3, exhibits a pseudo-C_s-symmetric structure with an octahedrally-coordinated Ir(III) center, and a coordination sphere that is in line with the solution NMR data. As mentioned above, complex **4** is structurally very similar to **3**, as confirmed by its NMR data collected in CDCl₃. Thus, its ³¹P{¹H} NMR spectrum displays a singlet at 23.1 ppm, and its ¹H NMR spectrum contains hydride resonances that are reminiscent of complex **3**, i.e., two triplet-of-doublets signals at -22.90 ppm (²J_{PH} = 22.4 Hz, ²J_{HH} = 6.8 Hz) and -26.46 ppm (²J_{PH} = 16.9 Hz, ²J_{HH} = 6.8 Hz).

It is interesting to note that when [Ir(ethylene)₂Cl]₂ was replaced by either [Ir(COD)Cl]₂ (COD = η²,η²-1,5-cyclooctadiene) or [Ir(COE)₂Cl]₂, complex **3** could be obtained directly, without requiring the addition of H₂, by simply allowing AcrPNPⁱPr to react with 0.5 equiv of each precursor in THF, at a nominal temperature of 80 °C. The reaction involving [Ir(COD)Cl]₂ required 24 h of heating, whereas [Ir(COE)₂Cl]₂ was found to react much faster, requiring only 1 h of heating. This could be traced to the chelating nature of COD, which is expected to inhibit its exchange with the pincer ligand. In an attempt to identify the source of the hydride ligands in complex **3** that is generated from [Ir(COE)₂Cl]₂ or [Ir(COD)

[†] Throughout this manuscript, the term “nominal temperature” refers to the temperature of the oil bath used to heat the reaction vessel. The nominal temperature often differs from the actual temperature of the reaction mixture, due to solvent evaporation and reflux.



Scheme 3. Synthesis of AcrPNP-iridium complexes **1–4** through reaction of the pincer ligands AcrPNP^{iPr} and AcrPNPPh with the Ir(I) precursors $[\text{Ir}(\text{olefin})_n\text{Cl}]_2$ [olefin = ethylene ($n = 2$), COE ($n = 2$), COD ($\eta^2,\eta^2\text{-1,5-cyclooctadiene}$; $n = 1$)].

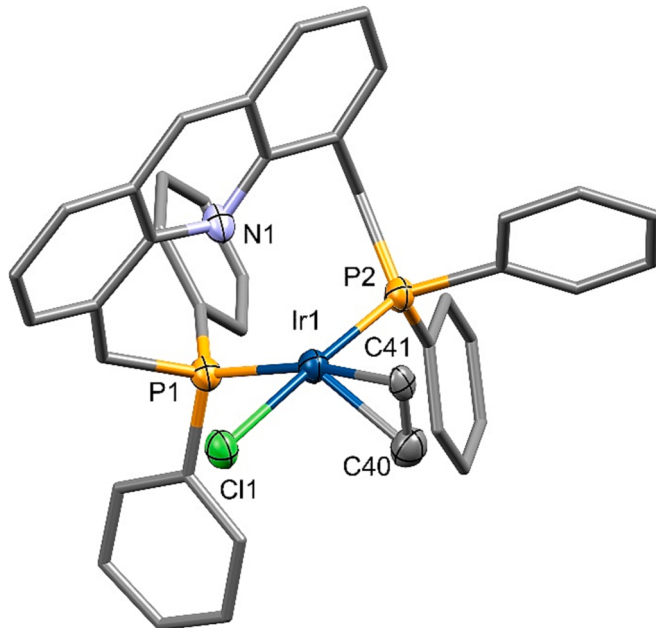


Fig. 2. Crystal structure of complex **2**. Atoms belonging to the first coordination sphere, as well as the acridine N donor, are presented as thermal ellipsoids (50% probability), whereas the rest of the structure is represented by capped sticks. All H atoms were omitted for clarity. Atoms are color coded as follows: Ir, blue; N, light blue; C, gray; P, orange; Cl, green; H, white. Select bond distances (Å) and angles (°): Ir1–P1, 2.328(1); Ir1–P2, 2.204(1); Ir1–Cl1, 2.408(1); Ir1–C41, 2.176(3); Ir1–C40, 2.111(4); C41–C40, 1.425(6); P2–Ir1–P1, 96.14(4); P2–Ir1–C41, 94.8(1); P2–Ir1–C40, 92.4(1); P1–Ir1–Cl1, 84.15(3); Cl1–Ir1–C41, 84.8(1); Cl1–Ir1–C40, 86.0(1); C41–Ir1–C40, 38.8(2).

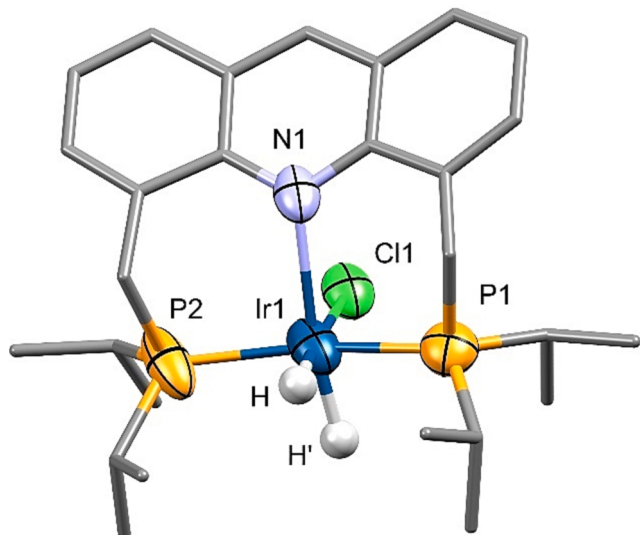


Fig. 3. Crystal structure of complex **3**. Atoms belonging to the first coordination sphere are presented as thermal ellipsoids (50% probability), whereas the rest of the structure is represented by capped sticks. An adventitious interstitial water molecule and all H atoms were omitted for clarity, except for the hydride ligands, which are represented by white spheres. These hydrides were located in the electron density map and their existence was corroborated by ¹H NMR spectroscopy. Atoms are color coded as follows: Ir, blue; N, light blue; C, gray; P, orange; Cl, green H, white. Select bond distances (Å) and angles (°): Ir1–Cl1, 2.457(1); Ir1–N1, 2.405(4); Ir1–P1, 2.268(2); Ir1–P2, 2.273(2); P2–Ir1–P1, 162.31(6); Cl1–Ir1–H, 176(2); P1–Ir–N1, 92.4(1); P2–Ir1–N1, 91.3(1); Cl1–Ir1–N1, 81.4(1); H–Ir1–H', 83(3).

$\text{Cl}]_2$, the reaction of each precursor with AcrPNP^{iPr} was repeated in THF and C_6D_6 , in the absence and presence of D_2O . Complex **3** was obtained in all of these experiments, but no deuterium was incorporated into it, indicating that the source of hydrides is the cycloalkene ligands, rather than the solvent or traces of water in the reaction mixture. It should be

noted that although **3** could be obtained in a single synthetic step from either $[\text{Ir}(\text{COE})_2\text{Cl}]_2$ or $[\text{Ir}(\text{COD})\text{Cl}]_2$, these routes could not afford it in pure form, unlike the two-step procedure involving $[\text{Ir}(\text{ethylene})_2\text{Cl}]_2$ and H_2 .

We have previously demonstrated that the Ru(II) complexes

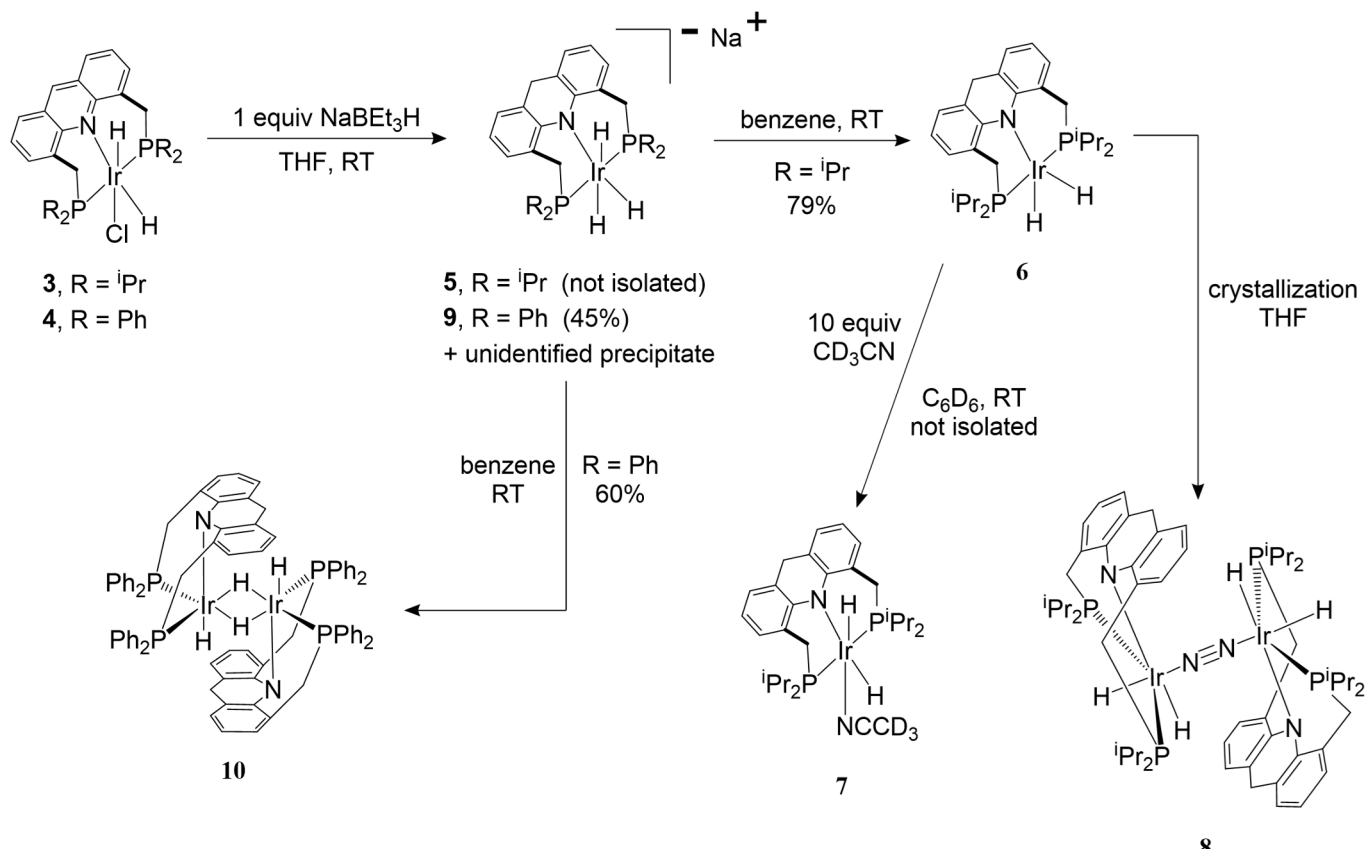
(AcrPNPⁱPr)Ru(H)(Cl)(CO) and (AcrPNPPh)Ru(H)(Cl)(CO), which are similar to **3** and **4**, react with NaBEt₃H to rapidly and selectively give the corresponding dearomatized acridanide variants (**Scheme 1**; R = ⁱPr, Ph) [8,9]. This prompted us to attempt the same transformation with the iridium complexes, as shown in **Scheme 4**. When complex **3** was treated with 1 equiv of NaBEt₃H in THF at room temperature, the ³¹P{¹H} NMR spectrum of the reaction mixture initially indicated the presence of two complexes, represented by two singlets, a broad one at 68.8 ppm and a narrow one at 62.2 ppm. Upon standing at room temperature, the complex associated with the higher-field resonance slowly gave way to the lower-field one, and the former also proved too unstable for isolation. However, repeating the reaction in THF-d₈ under closely-controlled conditions (see the Experimental Section), and conducting the NMR measurements at -20 °C, allowed us to generate this unstable species *in situ* as the only observable reaction product, fully characterize it at this low temperature, and identify it as the anionic dearomatized trihydrido Ir(III) complex **5** (**Scheme 4**). Its low-temperature ³¹P{¹H} NMR spectrum, which is practically identical to the room-temperature one, displays a singlet at 62.2 ppm, clearly indicating that its P-donors are symmetry-related, in accordance with the C_s symmetry of its proposed structure, having a mirror plane that contains the IrH₃ fragment and bisects the acridanide moiety. Its ¹H NMR spectrum exhibits two hydride resonances with a 2:1 integral ratio, i.e., a multiplet at -13.02 ppm representing the two mutually *trans* hydrides, and a multiplet at -23.56 ppm belonging to the third hydride, which is coupled to the former two, as demonstrated by a ¹H COSY experiment. Similar hydride NMR patterns have been reported previously for pincer complexes of the general type (PNP)Ir(H)₃ bearing mutually *trans* hydrides [36–38]. In addition, the low-field aromatic methine signal associated with the acridine C9 position of the parent complex **3** gave way to two mutually-coupled resonances, at 3.89 and 3.64 ppm (²J_{HH} = 16.5 Hz), attributed to a benzylic methylene group, indicating that the central ring of the acridine backbone had been dearomatized, turning it into an acridanide moiety. This was further supported by the appearance of the respective methylene resonance at 35.6 ppm in the ¹³C{¹H} NMR spectrum. The ²³Na NMR spectrum of **5** in THF, at room temperature, showed no observable signal, but upon addition of 18-crown-6 (2 equiv vs complex **3**), which is known to strongly coordinate Na⁺ [39,40], a broad singlet appeared at -9.8 ppm ($\Delta\nu_{1/2}$ = 492 Hz). This is comparable to previously reported solution ²³Na NMR data for the complex [(18-crown-6)Na]⁺ [41], thereby confirming the presence of a sodium cation, and indicating that complex **5** itself is negatively charged. The absence of a ²³Na NMR signal prior to the addition of crown ether suggests that Na⁺ is closely associated with the anionic complex **5**, rather than being fully solvated by THF, since the ²³Na NMR spectra of NaBEt₃H or NaBAr_f (BAr_f = tetrakis[3,5-bis(trifluoromethyl)phenyl]borate) in THF display distinct singlets at -3.3 and -6.6 ppm, respectively. Finally, as noted in **Scheme 4**, the generation of complex **5** from **3** and 1 equiv of NaBEt₃H was accompanied by a significant amount of solid precipitate. Apart from the expected NaCl, obtained by hydride-induced chloride abstraction from **3**, analysis of the solids using inductively-coupled plasma optical emission spectrometry (ICP-OES) revealed notable amounts of iridium and phosphorus, as well as some boron. This suggests the presence of unidentified iridium complexes in the precipitate, which could account for the incomplete mass balance of the reaction, as it is depicted in **Scheme 4**. It is important to note that when complex **3** was treated with 2 equiv of NaBEt₃H, instead of only one, a similar outcome was observed, with complex **5** being generated in solution alongside a substantial amount of solid precipitate.

As noted above, mixing equimolar amounts of complex **3** and NaBEt₃H in THF, at room temperature, afforded complex **5** alongside another iridium species. Furthermore, when the aforementioned low-temperature THF-d₈ solution of **5** was warmed to room temperature, it converted into the same new species within several hours, giving rise to a broad singlet at 68.6 ppm ($\Delta\nu_{1/2}$ = 206 Hz) in the ³¹P{¹H} NMR spectrum. The ¹H NMR spectrum displayed two broad singlets, at -26.89

and -28.18 ppm ($\Delta\nu_{1/2}$ = 301 and 123 Hz, respectively), representing two hydrides. We were able to synthesize this species directly in 79% yield, and identify it as the neutral dearomatized dihydrido Ir(III) complex **6** (**Scheme 4**). Although this complex is decidedly more stable than **5**, it was found to decompose in solution over time, and therefore its NMR characterization was carried out at -30 °C. At this low temperature, its ¹H and ³¹P{¹H} NMR spectra in THF-d₈ varied only slightly relative to room temperature, with the phosphines being represented by a broad singlet at 67.0 ppm ($\Delta\nu_{1/2}$ = 90 Hz), and the hydrides by broad singlets at -26.92 and -27.57 ppm ($\Delta\nu_{1/2}$ = 86 and 121 Hz, respectively). These NMR data suggest a trigonal-bipyramidal (TBP) coordination geometry for complex **6**, within an overall C_s-symmetric structure, wherein the chemically equivalent P-donors occupy the axial positions perpendicular to the molecular reflection plane. The highly negative hydride chemical shifts are comparable to those of previously reported (PNP)Ir(H)₂ complexes bearing pincer ligands that are structurally and electronically similar to AcrPNPⁱPr, which were assigned TBP configurations [42–44]. As in the case of complex **5**, the structure of **6** features a reduced acridanide backbone, as indicated by the NMR signals associated with the C9 position of this N-heterotricyclic moiety. Thus, its low-temperature ¹H NMR spectrum exhibits two mutually-coupled doublets at 3.72 and 3.58 ppm (²J_{HH} = 14.7 Hz), each representing one hydrogen atom of the benzylic CH₂ group, and its corresponding ¹³C{¹H} NMR signal is a singlet at 35.6 ppm. The process by which **5** transforms into **6** is unclear, but we were able to detect H₂ gas above the reaction mixture, suggesting that **5** loses a hydride ligand through reaction with an unidentified proton source.

The fact that complex **6** displays broad phosphorus and hydride NMR signals in THF-d₈ is indicative of structural fluxionality in solution. This could be, for example, the result of reversible coordination of solvent molecules to the metal center, or dynamic isomerization of the TBP configuration into energetically-close structures, like the square-pyramidal one. Broad phosphorus and hydride singlets were also observed when the NMR spectra of **6** were recorded in C₆D₆ at room temperature, with their chemical shifts being very similar to those measured in THF-d₈, namely, 68.1 ppm for the P-donors, and -26.52 and -27.99 ppm for the hydrides. However, the fluxionality of this complex was inhibited when excess CD₃CN (~10 equiv) was added to this solution, thereby generating the corresponding acetonitrile adduct, complex **7** (**Scheme 4**). This complex, which was fully characterized *in situ* by NMR spectroscopy, displays sharp resonances in both the ¹H and ³¹P{¹H} spectra at room temperature, in contrast to **6**. Thus, the phosphine donors of **7** give rise to a narrow singlet at 60.3 ppm in the ³¹P{¹H} NMR spectrum, and the two hydride ligands are represented by sharp triplet-of-doublets signals in the ¹H NMR spectrum, at -22.43 ppm (²J_{PH} = 15.7 Hz, ²J_{HH} = 6.9 Hz) and -22.90 ppm (²J_{PH} = 19.1 Hz, ²J_{HH} = 6.9 Hz). Judging by the small ³¹P-¹H and ¹H-¹H coupling constants, these hydrides are *cis* to each other, as well as to the two chemically equivalent P-donors. Moreover, their NMR resonances are pushed significantly downfield relative to the hydrides in complex **6**, indicating that they are now positioned *trans* to the N-donors within the first coordination sphere, namely, acetonitrile and the acridanide moiety. All in all, the NMR data are consistent with an octahedral arrangement around the Ir(III) center of complex **7**, with the pincer ligand maintaining its meridional coordination, and the whole structure retaining the C_s symmetry of **6**. It is noteworthy that when the solution containing **7** was placed under reduced pressure to remove all volatiles, and the resulting solids were redissolved in C₆D₆, complex **6** was fully regenerated. Hence, even though complex **7** appears to be nonfluxional in the presence of excess acetonitrile, coordination of this ligand is reversible, and it can be easily pumped off [37].

Another notable observation was made when we attempted to crystallize complex **6** from THF, under various conditions. Different samples yielded X-ray-quality crystals, but they were repeatedly found to be those of the dimeric N₂-bridged complex **8** (**Scheme 4**; see Figure S79 for the crystal structure), rather than the monomeric



Scheme 4. Reaction of complexes **3** and **4** with NaBET₃H and reactivity of the resulting products.

structure derived from the solution NMR data. Dinuclear Ir(III) complexes featuring bridging dinitrogen ligands are known, but are uncommon [43,45–49]. In order to explore the possibility that complex **6** was misidentified, and that it is, in fact, the abovementioned N₂-bridged dimer, we repeated the reaction of **3** with NaBET₃H in THF under an atmosphere of ¹⁵N₂ (98 atom% ¹⁵N). However, upon formation of the Ir(III) dihydride complex, as determined by ³¹P{¹H} NMR spectroscopy, the room-temperature ¹⁵N{¹H} spectrum of the solution simply revealed the presence of dissolved ¹⁵N₂ (a singlet at 309.6 ppm), with no other ¹⁵N-labeled species being observed. Furthermore, diffusion-ordered ¹H NMR spectroscopy (¹H-DOSY) experiments, conducted using THF-d₈/THF (1.0:5.5 v/v) as solvent, showed that the diffusion coefficient of the complex identified as **6** is highly comparable to that of the monomeric complex **3**, i.e., 0.953(2) × 10⁻⁹ vs 0.918(6) × 10⁻⁹ m²/s, respectively. Combined together, the results of these ¹⁵N-labeling and ¹H-DOSY experiments confirm that complex **6** is monomeric, and does not contain a bridging dinitrogen ligand. It therefore appears that complex **8** is but a minor species in solution, which crystallizes preferentially.

Complex **4**, which is structurally analogous to **3**, reacted in THF, at room temperature, with 1 equiv of NaBET₃H to give two new complexes, represented in the ³¹P{¹H} NMR spectrum by sharp singlets at 48.8 and 20.1 ppm. As was observed for complex **3**, one of these new species – here associated with the lower-field resonance – gradually transformed into the second (higher-field) species. However, the former could be isolated in 45% yield, and was fully characterized by NMR spectroscopy in THF-d₈ at -20 °C, thereby allowing its identification as complex **9** (Scheme 4), the Ph-substituted variant of **5**. At this low temperature, the phosphine donors of **9** gave rise to a sharp singlet at 49.4 ppm in the ³¹P{¹H} NMR spectrum. Its ¹H NMR spectrum displayed two high-field multiplets, one at -11.75 ppm, corresponding to two mutually *trans* hydrides, and another at -21.92 ppm, attributed to a third hydride positioned *cis* to them. As was observed for the transformation **3** → **5**, the

acridine backbone of **4** underwent dearomatization by NaBET₃H into the acridanide moiety found in **9**, as indicated by the conversion of the aromatic C9 position of the parent complex into a benzylic CH₂ moiety represented by two mutually-coupled ¹H NMR signals at 4.08 and 3.80 ppm (²J_{HH} = 16.9 Hz), as well as a ¹³C NMR signal at 34.2 ppm. Furthermore, the ²³Na NMR spectrum of **9** in THF featured a broad singlet at 12.3 ppm ($\Delta\nu_{1/2}$ = 744 Hz), which after addition of 18-crown-6 (0.6 equiv vs complex **9**) gave way to a sharper singlet at -6.1 ppm ($\Delta\nu_{1/2}$ = 486 Hz). Comparing these NMR data with the abovementioned data for complex **5**, NaBET₃H and NaBAR_b, it can be concluded that **9** is an anionic Ir(III) complex bearing a sodium counterion.

As described above, complex **9** was accompanied by a second species, which was represented by the higher-field resonance in the ³¹P{¹H} NMR spectrum and became dominant over time, as the THF solution was allowed to stand at room temperature. Under these conditions, this transformation would normally proceed very slowly, over many days. Nevertheless, we were able to quickly and selectively obtain the new species as the sole product by using a simply-modified procedure, namely, mixing equimolar amounts of complex **4** and NaBET₃H in THF, but pumping the solvent off after only 30 min at room temperature, and then extracting the remaining solid residue with benzene. Full characterization of this compound revealed it to be the dimeric complex **10** (Scheme 4), which we were able to isolate in 60% yield. It should also be noted that when complex **9** was dissolved in benzene, it transformed into **10** in a matter of minutes at room temperature, thereby highlighting the role of benzene in the selective synthesis of **10** described above. As with the conversion of **5** into **6**, the mechanism by which complex **9** transforms into **10** is unclear, but it is evident that the reaction generates notable amounts of insoluble solids containing unidentified iridium complexes, as judged by the presence of iridium, phosphorus and boron in the precipitate, determined by ICP-OES.

The dimeric nature of complex **10** was first revealed by its crystal

structure (see below), but this was also confirmed to be the case in solution through an ^1H -DOSY experiment conducted in THF-d₈/THF (1.0:5.5 v/v). Thus, the diffusion coefficient of this complex, at $0.606(6) \times 10^{-9} \text{ m}^2/\text{s}$, is 64% that of monomeric complex **6**, indicating that the average diameter of **10** is significantly larger than that of **6**. The fact that the $^{\text{i}}\text{Pr}$ -substituted species (**6**) remains monomeric in solution, whereas the Ph-substituted one (**10**) favors dimerization is intriguing, and may be due to steric hindrance by the $^{\text{i}}\text{Pr}$ substituents, which are bulkier than the Ph ones (for comparison, the Tolman cone angles of $\text{PMe}({}^{\text{i}}\text{Pr})_2$ and PMePh_2 in octahedral complexes are 160 and 142°, respectively [50]).

The proposed solution structure of complex **10**, as shown in Scheme 4, belongs to point group C_{2h} , with a mirror plane that is perpendicular to the $\text{Ir}_2(\mu\text{-H})_2$ core and contains the two metal centers, and a C_2 axis that passes through the two bridging hydrides. The $^{31}\text{P}\{\text{H}\}$ NMR spectrum of this complex in C₆D₆ exhibits a singlet at 20.1 ppm, which, as would be expected from the molecular symmetry, represents all four chemically-equivalent phosphine donor groups of the two pincer ligands within the dimer. Its ^1H NMR spectrum displays two 1:1 multiplets, at -7.98 and -13.94 ppm, which arise from the hydride ligands. Assisted by the corresponding ^{31}P -decoupled ^1H NMR spectrum, we assigned the lower-field resonance, which features a large two-bond ^{31}P - ^1H coupling constant of 66.5 Hz and a small ^1H - ^1H coupling constant of only 3.6 Hz, to the two symmetry-related bridging hydrides. Each of these hydrides is situated *trans* to two P-donors, one from each monomeric complex, leading to the large value of $^{2}J_{\text{PH}}$, whereas the remaining phosphines and terminal hydrides are all situated *cis* to them, resulting in much smaller coupling constants (e.g., $^{2}J_{\text{HH}}$ cited above). A large ^{31}P - ^1H coupling constant of 65 Hz was previously reported for the *trans*-P-Ir-H fragments of a structurally-similar hydride-bridged dimeric Ir(III) complex bearing pyrrolide-based PNP-type pincer ligands [51]. The two

terminal hydrides of **10**, which are also symmetry-related, are represented by the ^1H resonance near -14 ppm that appears as a broadened singlet, and must therefore feature a small $^{2}J_{\text{PH}}$ value of only a few Hz, as expected of hydrides that are situated *cis* to the P-donors. The fact that the bridging hydrides are *trans* to the phosphine groups is consistent with facial coordination of the pincer ligands in **10**. These ligands retain the dearomatized acridanide backbone observed in complex **9**, as indicated by the characteristic NMR peaks of the methylene group at the C9 position (5.30 and 4.20 ppm in the ^1H NMR spectrum, 37.3 ppm in the $^{13}\text{C}\{\text{H}\}$ NMR spectrum).

Crystals of complex **10** suitable for X-ray diffraction were grown at room temperature from a THF solution overlaid with pentane. The molecular structure of this complex, which co-crystallized with THF molecules in the space group $P2_1/n$, is depicted in Fig. 4. It should be noted that despite the presence of many arene groups in **10**, no significant intra- or intermolecular π - π stacking is observed in its crystal structure. The dimeric structure of this complex, which belongs to point group C_i , is comprised of two (PNP)IrH₂ units, symmetry-related through an inversion point halfway between the Ir(III) centers, and interlinked via two bridging hydride ligands. In solution, this low-symmetry structure is no longer subject to crystal lattice constraints, and the molecular motions of the inherently flexible acridanide pincer ligand are expected to average out on the NMR timescale, thereby effectively increasing the symmetry to C_{2h} . In line with the solution NMR data, each metal center in the crystal structure exhibits an octahedral coordination geometry, defined by three hydride ligands – one of which is terminal (and all of which were located in the electron density map) – and a facially-coordinated pincer ligand, the donor atoms of which are positioned *trans* to all hydrides. To the best of our knowledge, only one such dimeric PNP-Ir(III) complex has been reported previously, namely,

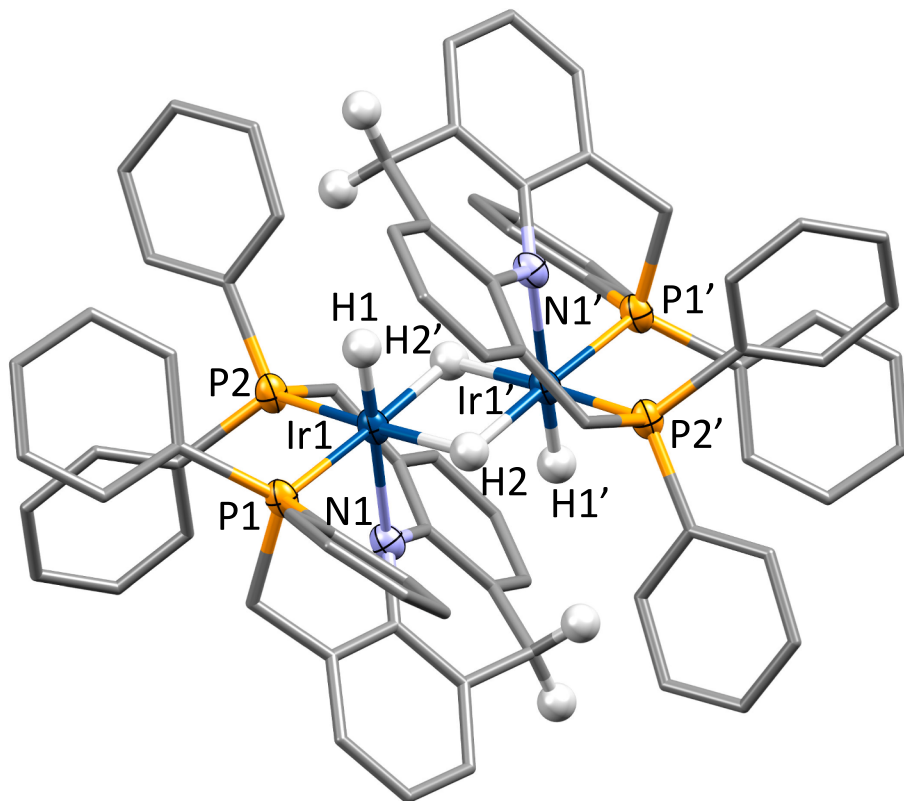
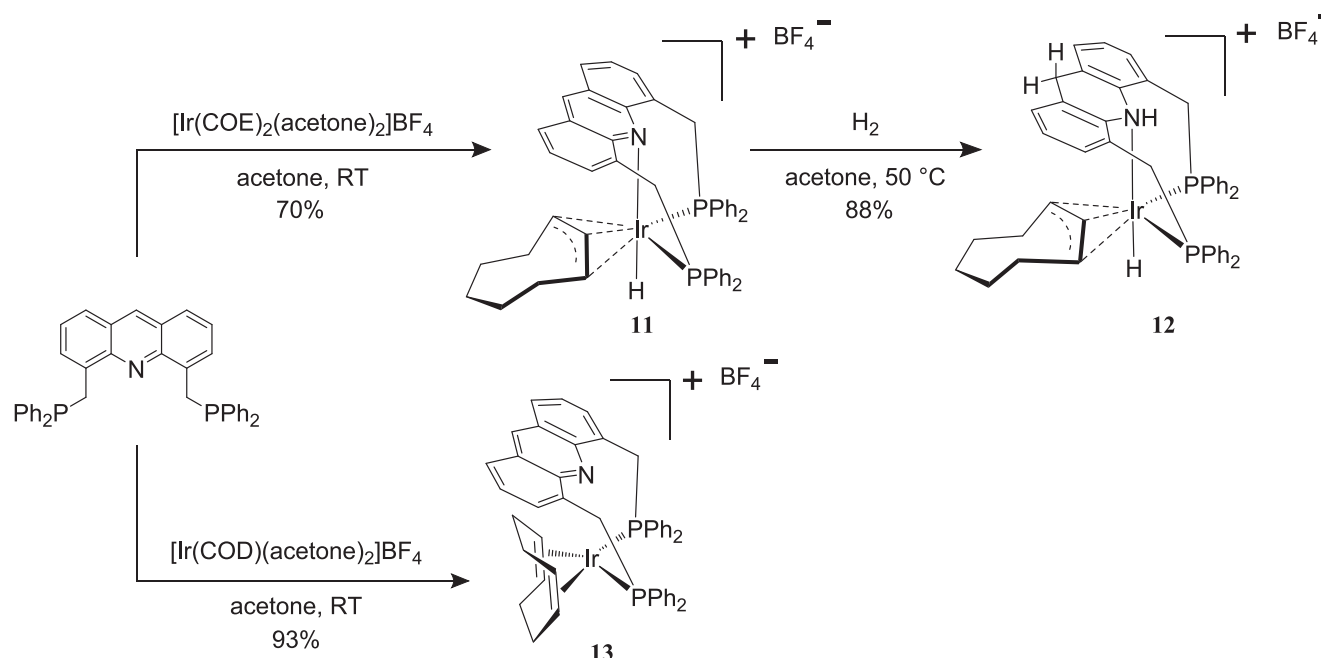


Fig. 4. Crystal structure of complex **10**. Atoms belonging to the first coordination sphere are presented as thermal ellipsoids (50% probability), whereas the rest of the structure is represented by capped sticks. Two interstitial THF molecules and all H atoms were omitted for clarity, except for the hydride ligands and H atoms at the C9 position of each acridanide ligand. The displayed hydrogen atoms (white spheres) were located in the electron density map and their existence was corroborated by ^1H NMR spectroscopy. Atoms are color coded as follows: Ir, blue; N, light blue; C, gray; P, orange; H, white. Select bond distances (Å) and angles (°): Ir1-N1, 2.228(4); Ir1-P1, 2.217(1); Ir1-P2, 2.250(1); P1-Ir1-P2, 95.42(4); N1-Ir1-P1, 91.9(1); N1-Ir1-P2, 79.9(1).



Scheme 5. Synthesis of cationic AcrPNPPh-iridium complexes **11–13** through reaction of the pincer ligand AcrPNPPh with the Ir(I) precursors $[\text{Ir}(\text{olefin})_n(\text{acetone})_2]\text{BF}_4$ [$\text{olefin} = \text{COE}$ ($n = 2$), COD ($n = 1$)].

the abovementioned complex featuring a pyrrolide-based PNP ligand [51]. It displays first coordination spheres that are comparable to **10**, including an $[\text{Ir}(\text{H})(\mu\text{-H})_2]$ core structure, but each of its two pincer ligands is bridging, spanning both metal centers, in contrast to **10**. It is noteworthy that although each monomer comprising complex **10** is reminiscent of **6**, the pincer ligands in these two complexes exhibit different coordination geometries, i.e., facial vs meridional, and this attests to the flexibility of the acridanide-based pincer ligands.

In addition to the neutral Ir(I) precursors $[\text{Ir}(\text{olefin})_n\text{Cl}]_2$ [olefin = ethylene ($n = 2$), COE ($n = 2$), COD ($n = 1$)], which, together with the ligands AcrPNPⁱPr and AcrPNPPh, afforded the abovedescribed series of neutral and anionic complexes, we have also studied the reactions of the cationic precursors $[\text{Ir}(\text{COE})_2(\text{acetone})_2]\text{BF}_4$ [52] and $[\text{Ir}(\text{COD})(\text{acetone})_2]\text{BF}_4$ [53] with AcrPNPPh (Scheme 5). Both precursors were prepared *in situ* by treating either $[\text{Ir}(\text{COE})_2\text{Cl}]_2$ or $[\text{Ir}(\text{COD})\text{Cl}]_2$ with 2 equiv of AgBF_4 in acetone.

Upon mixing $[\text{Ir}(\text{COE})_2(\text{acetone})_2]\text{BF}_4$ with 1 equiv of AcrPNPPh in acetone, full conversion was observed within minutes at room temperature, leading to a single product, represented by a singlet at 21.3 ppm in the $^{31}\text{P}\{\text{H}\}$ NMR spectrum. Isolation and full characterization of this compound revealed that it is not simply a cationic PNP-supported Ir(I)-olefin adduct, somewhat similar to complex **2**, but rather the Ir(III) complex **11** (Scheme 5), featuring an η^3 -cyclooctenyl ligand, alongside a hydride and the pincer ligand itself. This compound, which was isolated in 70% yield, is essentially the product of intramolecular C—H activation of a coordinated COE molecule. Complexes exhibiting the $\text{Ir}(\text{H})(\eta^3\text{-cyclooctenyl})$ fragment, stabilized by various ligand platforms and generated through such C—H activation, have been reported previously [54–60].

The $^{31}\text{P}\{\text{H}\}$ NMR spectrum of **11** in acetone- d_6 displays a singlet at 21.3 ppm, as mentioned above, representing its two chemically-equivalent phosphine donors. This is consistent with the proposed C_s -symmetric structure of this complex, which has a reflection plane that bisects the P—Ir—P angle, acridine backbone and cyclooctenyl ligand. In the ^1H NMR spectrum, this cyclooctenyl moiety gives rise to two mutually-coupled methine signals, i.e., a multiplet at 2.42 ppm and a triplet at -0.05 ppm ($^3J_{\text{HH}} = 8.2$ Hz), with a 2:1 integral ratio, which belong to the flanking and central hydrogen atoms of its coordinated

π-allyl fragment, respectively. The corresponding $^{13}\text{C}\{\text{H}\}$ NMR peaks of these methines are a doublet at 62.4 ppm ($^2J_{\text{CP}} = 29.1$ Hz) and a singlet at 104.7 ppm. Similarly-sized ^{31}P — ^{13}C coupling constants were observed for cationic Ir(III) complexes bearing an η^3 -cyclooctenyl ligand *trans* to phosphine donor groups [61], indicating an analogous arrangement in complex **11**. This, in turn, implies that the pincer ligand in **11** is facially coordinated to the iridium center, with its two phosphine donors positioned *cis* to each other. The hydride ligand of this complex is represented in the ^1H NMR spectrum by a triplet at -27.50 ppm ($^2J_{\text{PH}} = 15.6$ Hz). Finally, the BF_4^- counterion gives rise to a sharp singlet at -151.6 ppm in the $^{19}\text{F}\{\text{H}\}$ NMR spectrum, which is characteristic of a non-coordinating tetrafluoroborate ion.

X-ray-quality crystals of complex **11** were isolated from an acetone solution overlaid with pentane and kept at room temperature, and its solid-state structure is shown in Fig. 5. The complex, which co-crystallized with acetone molecules in the triclinic space group $P\bar{1}$, displays a formally octahedral coordination geometry, with a facially-coordinated pincer ligand, an η^3 -cyclooctenyl ligand *trans* to the two phosphine donors, and a hydride *trans* to the acridine N-donor. The BF_4^- counterion is outer-sphere, in line with the solution $^{19}\text{F}\{\text{H}\}$ NMR data. It should be noted that two of the four phenyl substituents on the P-donors in complex **11**, one from each donor group, appear to be π-stacked, as can be seen in Fig. 5, and as indicated by the existence of numerous short contacts between their respective carbon atoms.[§] The manner in which all four phenyl groups are tilted breaks the molecular symmetry of the solid-state structure of this complex, which would otherwise be C_s -symmetric, as proposed for the solution phase.

Despite the fact that complex **11** is a saturated Ir(III) species, it was found to react with excess hydrogen gas (2 bar) in acetone at 50 °C. This behavior is reminiscent of complex **1**, but in the present case H_2 did not oxidatively add to the metal center. Instead, it was found to add across the central ring of the acridine scaffold of the pincer ligand, thereby affording the dearomatized acridane-based complex **12** (Scheme 5). This compound, which was isolated in 88% yield, was fully characterized by

[§] A short contact is defined as a nonbonding interatomic distance that is smaller than or equal to the sum of vdW radii of the interacting atoms.

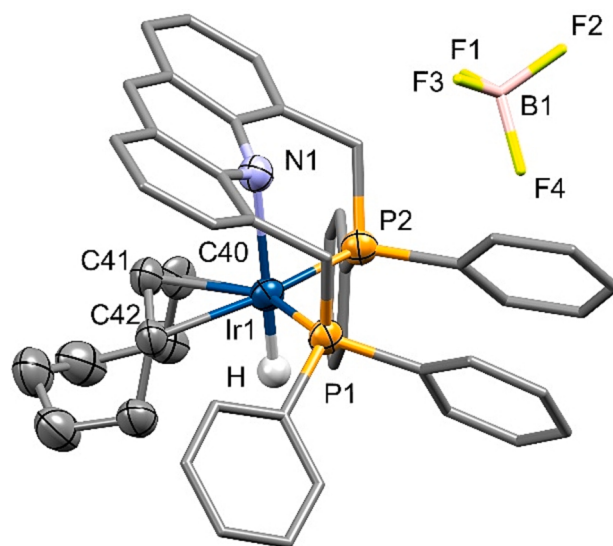


Fig. 5. Crystal structure of complex **11**. Atoms belonging to the first coordination sphere and the cyclooctenyl ligand are presented as thermal ellipsoids (50% probability), whereas the rest of the structure is represented by capped sticks. The BF_4^- counterion is disordered and only those B and F atoms with largest site occupancy (73%) are shown. Three interstitial acetone molecules and all H atoms were omitted for clarity, except for the hydride ligand. This hydride (white sphere) was located in the electron density map and its existence was corroborated by ^1H NMR spectroscopy. Atoms are color coded as follows: Ir, blue; N, light blue; C, gray; P, orange; B, pink; F, yellow; H, white. Select bond distances (\AA) and angles ($^\circ$): Ir1–P1, 2.265(2); Ir1–P2, 2.283(2); Ir1–N1, 2.363(6); Ir1–C41, 2.166(6); Ir1–C42, 2.278(6); Ir1–C40, 2.296(5); C40–C41, 1.41(1); C41–C42, 1.42(1); N1–Ir1–P2, 88.0(1); N1–Ir1–P1, 90.6(1); N1–Ir–C42, 97.7(2); N1–Ir–C41, 81.0(2); N1–Ir1–C40, 96.1(2); C40–C41–C42, 124.3(7).

NMR spectroscopy and X-ray crystallography, demonstrating that, apart from the dearomatization, it retains the C_s -symmetric structure of the parent complex **11**. Its $^{31}\text{P}\{^1\text{H}\}$ NMR spectrum in acetone- d_6 exhibits a singlet at 23.7 ppm, representing the two chemically equivalent phosphine donors, and its hydride ligand gives rise to a triplet at –25.74 ppm ($J_{\text{PH}} = 15.9$ Hz). The fact that the acridine moiety of **11** had been reduced into acridane was established by the disappearance of the singlet at 9.70 ppm in the ^1H NMR spectrum of **11**, attributed to the methine hydrogen atom at the acridine C9 position, and appearance of two mutually-coupled 1:1 doublets at 4.80 and 4.52 ppm ($J_{\text{HH}} = 21.7$ Hz), ascribed to two methylene hydrogen atoms at the very same position in complex **12**. This structural change was also apparent in the $^{13}\text{C}\{^1\text{H}\}$ NMR spectrum, as the arene resonance of position C9 at 145.8 ppm gave way to a benzylic methylene peak at 30.3 ppm. Moreover, the presence of an acridane N–H bond in complex **12** was corroborated by its solid-state infrared spectrum, which displays a characteristic N–H stretching band at 3255 cm^{-1} that is missing from the corresponding spectrum of **11**. It should be noted that the observed downfield shift of the hydride NMR signal, from –27.50 ppm in **11** to –25.74 ppm in **12**, may reflect an increase in donor strength upon going from the sp^2 -hybridized N atom of acridine to the sp^3 -hybridized N atom of acridane.

The molecular architecture of complex **12** was further confirmed by examining its crystal structure, which is depicted in Fig. 6, and is based on X-ray diffraction data from crystals grown in an acetone solution overlaid with pentane and stored at room temperature. Complex **12**, like its precursor **11**, co-crystallized with acetone molecules in the space group $P\bar{1}$. More importantly, overlaying the molecular structures of these complexes revealed that they are essentially identical, except for the acridine-derived tricyclic core, in which variations are visibly apparent. Particularly telling are the changes associated with the C9 position and the nitrogen donor atom. First, each of these two atoms

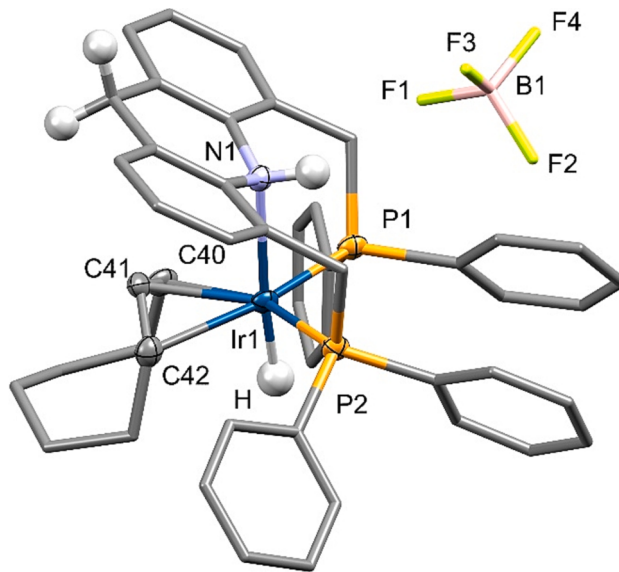


Fig. 6. Crystal structure of complex **12**. Atoms belonging to the first coordination sphere are presented as thermal ellipsoids (50% probability), whereas the rest of the structure is represented by capped sticks. The BF_4^- counterion is disordered and only those B and F atoms with largest site occupancy (60%) are shown. Three interstitial acetone molecules and all H atoms were omitted for clarity, except for the hydride ligand, hydrogen atoms at the C9 position and N–H moiety. The displayed hydrogen atoms (white spheres) were located in the electron density map and their existence was corroborated by ^1H NMR and IR spectroscopies. Atoms are color coded as follows: Ir, blue; N, light blue; C, gray; P, orange; B, pink; F, yellow; H, white. Select bond distances (\AA) and angles ($^\circ$): Ir1–C42, 2.264(4); Ir1–C41, 2.147(4); Ir1–C40, 2.287(3); Ir1–N1, 2.340(3); Ir1–P1, 2.285(1); Ir1–P2, 2.281(1); C40–C41, 1.409(5); C41–C42, 1.400(5); P2–Ir1–P1, 106.97(3); P2–Ir1–N1, 89.03(7); P1–Ir1–N1, 87.08(7); P2–Ir1–C42, 94.6(1); P2–Ir1–C41, 127.0(1); P1–Ir1–C40, 92.0(1); P1–Ir1–C41, 124.6(1); C40–Ir1–C41, 36.9(1); C41–Ir1–C42, 36.9(1); N1–Ir1–C41, 82.7(1).

carries a new hydrogen atom that was located in the electron density map and is absent in **11**. Second, the geminal C–C and C–N bonds emanating from these atoms undergo elongation upon going from structure **11** to **12**, namely, $\bar{d}(\text{C–C})$ increases from 1.40(1) to 1.49(1) \AA , and $\bar{d}(\text{C–N})$ increases from 1.35(1) to 1.44(1) \AA . This is consistent with the rehybridization of the carbon and nitrogen atoms, from sp^2 to sp^3 , upon hydrogenation of the central ring of the acridine scaffold. It is noteworthy that the acridane N–H bond appears to be engaged in hydrogen bonding with the BF_4^- counterion, as indicated by the existence of a short N–F contact in the crystal structure of **12**, which is not observed in **11** [the shortest N–F distance in **12** is 2.97(1) \AA , which is smaller than the sum of the respective vdW radii, $r_N + r_F = 3.12\text{ \AA}$; the corresponding N–F distance in **11** is 3.47(2) \AA]. It should be further noted that the $^{19}\text{F}\{^1\text{H}\}$ NMR spectrum of **12** in acetone exhibits a sharp singlet at –153.0 ppm, indicating that the BF_4^- counterion is not engaged in significant hydrogen bonding in this solvent, nor is it coordinated to the metal center.

The 1,4-addition of H_2 to the *N*-heterocyclic backbone of complex **11** is unprecedented for complexes of acridine- or pyridine-based pincer ligands, to the best of our knowledge. However, it is reminiscent of the reactivity observed for the abovementioned Ru(II) complex ($\text{AcrPNP}^{\text{i}}\text{Pr}$) $\text{Ru}(\text{H})(\text{Cl})(\text{CO})$. As was reported previously, when this complex was treated with excess H_2 in refluxing toluene, in the presence of base, it converted into the dearomatized complex ($\text{AcrPNP}^{\text{i}}\text{Pr}^*$) $\text{Ru}(\text{H})(\text{CO})$ (Scheme 1) [13]. Using D_2 instead of H_2 , we were able to demonstrate that dihydrogen formally adds across the metal–ligand framework, being split between the C9 position and the Ru(II) center. This was computationally shown to take place through a d^8 Ru(0) intermediate

that oxidatively adds H₂, followed by long-range hydrogen transfer from the metal center to the C9 position. Based on this mechanism, we propose an analogous pathway for the present iridium system, as illustrated in **Scheme 6**. It is reasonable to assume that **11** undergoes C—H reductive elimination upon heating, thereby affording the respective d⁸ Ir(I)-COE complex (intermediate A; **Scheme 6**). This, in turn, is isoelectronic to the aforementioned Ru(0) species, and may react analogously, with initial oxidative addition of H₂ to yield an Ir(III) dihydride species (**B**), followed by hydrogen transfer to the C9 position. The remaining hydride ligand could then transfer to the nitrogen atom as a proton, thereby regenerating the Ir(I) center (**C**), which could convert the coordinated COE back into its η³-cyclooctenyl form through C—H activation.

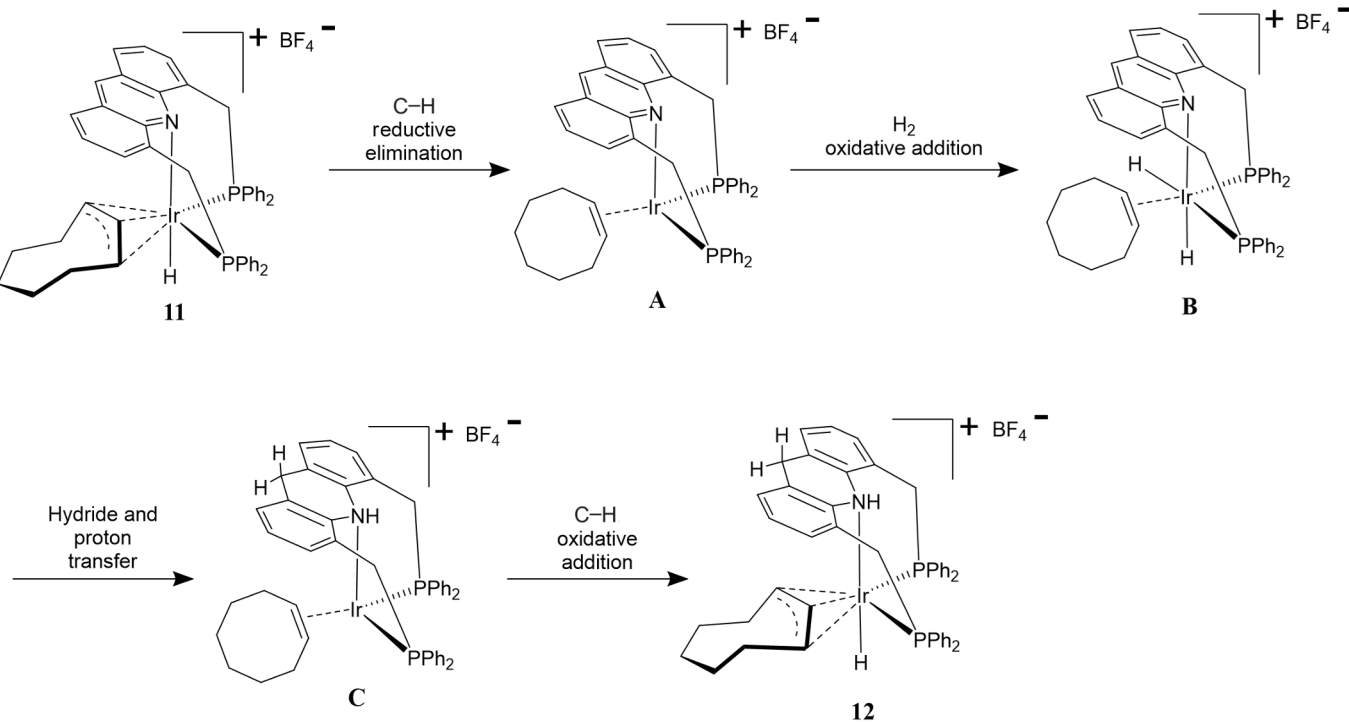
Replacing the olefin ligand in the cationic Ir(I) precursor, from the monodentate COE to the bidentate COD, resulted in a markedly different outcome. Thus, mixing [Ir(COD)(acetone)₂]BF₄ with AcrPNPPh in acetone, at room temperature, afforded the cationic Ir(I) complex **13** (**Scheme 5**), which was isolated in 93% yield, and the structure of which resembles compound **2**. The ³¹P{¹H} NMR spectrum of **13** in acetone-d₆ shows a singlet at 11.9 ppm, representing two chemically equivalent phosphine donors, in line with the proposed C_s-symmetric structure of this complex, which has a mirror plane that bisects the P—Ir—P angle, acridine backbone and cyclooctadiene ligand. The ¹H NMR data clearly indicate that **13** exhibits an intact COD ligand, with no C—H activation being detected, in marked contrast to **11**. Nevertheless, it appears that coordination of COD is fluxional at room temperature, as suggested by the number of ¹H and ¹³C NMR resonances associated with this ligand. Thus, had this ligand been strongly-coordinated, at least four ¹H peaks would be expected, as well as the same number of ¹³C peaks, but their actual number is half that. Moreover, the four olefinic hydrogen atoms of COD are represented by a sharp singlet at 3.46 ppm, indicating that all of them are chemically equivalent and effectively decoupled from the aliphatic hydrogens. Similarly, the four olefinic carbon atoms give rise to only one ¹³C{¹H} NMR peak, a triplet at 79.0 ppm (²J_{CP} = 6.3 Hz), showing that these chemically-equivalent atoms are coupled to both P-donors of the pincer ligand. These ¹H and ¹³C NMR peaks are shifted substantially upfield relative to solvated COD, for which δ(¹H) = 5.51 ppm and δ(¹³C) = 129.2 ppm in acetone-d₆ at room temperature [62],

thereby indicating the existence of notable Ir → C=C backbonding in the COD complex. Interestingly, the ¹H and ¹³C{¹H} NMR spectra of **13**, including the COD resonances, remain essentially unchanged even at -40 °C.

The molecular structure of **13** was confirmed by X-ray crystallographic analysis of an appropriate crystal grown from an acetone solution overlaid with pentane, which was kept at room temperature. The complex, which crystallized in the monoclinic space group P2₁/c, displays a square-planar coordination geometry and an outer-sphere BF₄⁻ counterion, as shown in **Fig. 7**. Within this coordination sphere, the COD ligand is expectedly *cis*-chelating, and the phosphine donors of the pincer ligand also assume a mutually *cis* configuration, as in complex **2**. In fact, the whole (AcrPNPPh)Ir fragment of **13** is essentially isostructural to that of **2**. This includes the close proximity between the metal center and acridine N-donor, which are separated by only 2.711 (3) Å, a distance that is over 30% shorter than the sum of vdW radii of the respective atoms. This, in turn, implies the existence of an Ir···N interaction, which should be promoted by the presence of the π-accepting COD ligand. Interestingly, the C=C bonds of this ligand differ significantly in length, at 1.342(9) and 1.398(7) Å. The shorter bond is virtually identical in length to that of free COD, 1.340(3) Å [63], whereas the longer bond is close to 1.38(2) Å, which is the average length calculated for coordinated COD in *cis*-[Ir(PR₃)₂(COD)]⁺ complexes, based on the 23 high-quality structures (*R* ≤ 0.05) found in the CSD. These data suggest that one of the COD C=C bonds in complex **13** exhibits considerable backdonation, whereas the other bond experiences little backbonding. This variation in metal-COD interactions is consistent with the fluxional coordination of this ligand, as deduced from the solution NMR results. It should be noted that the asymmetric crystal structure of **13** is expected to easily average out in solution, on the NMR timescale, giving an effectively C_s-symmetric structure, due to the innate flexibility of the acridine pincer ligand.

3. Conclusions

Acridine-based PNP-type pincer ligands, which were first reported over a decade ago, have thus far been used for the construction of a



Scheme 6. Proposed mechanism for the reaction of **11** with H₂ to form **12**.

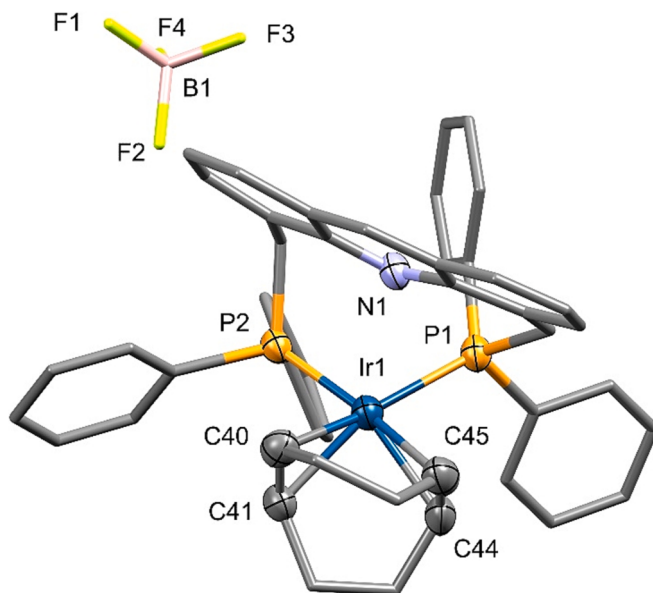


Fig. 7. Crystal structure of complex **13**. Atoms belonging to the first coordination sphere and the COD ligand are presented as thermal ellipsoids (50% probability), whereas the rest of the structure is represented by capped sticks. All H atoms were omitted for clarity. Atoms are color coded as follows: Ir, blue; N, light blue; C, gray; P, orange; B, pink; F, yellow. Select bond distances (\AA) and angles ($^{\circ}$): Ir1–C40, 2.164(5); Ir1–C45, 2.194(4); Ir1–C44, 2.173(4); Ir1–C41, 2.185(4); Ir1–P1, 2.356(1); Ir1–P2, 2.320(1); P2–Ir1–P1, 94.51(4); P1–Ir1–C45, 92.6(1); P1–Ir1–C44, 87.0(1); C40–Ir1–P2, 92.6(1); C41–Ir1–P2, 89.3(1); C45–Ir1–C44, 35.8(2); C45–Ir1–C40, 79.6(2); C40–Ir1–C41, 37.5(2).

limited number of transition metal complexes. Most attention has previously been given to a few Ru(II) complexes, which have been employed as homogenous catalysts for a range of sustainable organic reactions, but a handful of Mn(I), Rh(III) and Ir(III) complexes have also been reported. We have now significantly expanded the scope of known AcrPNP complexes by introducing a series of new Ir(I) and Ir(III) complexes of these ligands, which are described in the present report.

As detailed above, the new AcrPNP-Ir complexes were synthesized through different sequences of reactions, initially involving the pincer ligands AcrPNPⁱPr and AcrPNPPh, and various Ir(I)-olefin precursors. Some of these initial reactions resulted in intramolecular C–H activation, leading to Ir(III) complexes (**1**, **11**), whereas others gave Ir(I) complexes by simple ligand exchange (**2**, **13**). Most of these products were shown to activate H₂ gas, *via* either typical oxidative addition to the metal center, thereby affording dihydrido Ir(III) complexes (**3**, **4**), or through a unique 1,4-addition to the acridine backbone to give a dearomatized acridane-based complex (**12**). Furthermore, the aforementioned dihydride complexes were found to react with NaBEt₃H, resulting in the addition of two hydrides per complex, and leading to anionic dearomatized trihydrido Ir(III) complexes (**5**, **9**). These were found to be unstable in solution, each one losing a hydride ligand to afford a new dihydride complex, which is either a monomer (**6**) or a hydride-bridged dimer (**10**). The monomeric complex was shown to reversibly coordinate CH₃CN (**7**), and also form an uncommon N₂-bridged Ir(III) dimer (**8**) upon crystallization.

The new iridium complexes presented in this work, with their observed structures and reactivities, highlight the unique properties of the acridine-based PNP ligands. In these complexes, the phosphine side-arms of the pincer ligands function as either *cis* or *trans* chelators, which translates into *facial* or *meridional* coordination when the N-donor is also involved, thereby reflecting the inherent structural flexibility of these ligands. In addition, and perhaps more importantly, these ligands were shown to support both metal-centered reactivity, i.e., C–H and H–H oxidative addition, and ligand-centered reactivity, i.e., hydride- and H₂-

induced dearomatization. As we continue to explore transition metal complexes of acridine-based PNP ligands, these attributes provide us with valuable tools for the development of new catalytic systems.

4. Experimental

4.1. General procedures

All reactions involving the pincer ligands, iridium precursors and new iridium complexes were carried out under an atmosphere of purified nitrogen in an MBraun glovebox, or by using common Schlenk techniques, in glassware that was oven-dried prior to use. Commercially available reagents were reagent grade or higher purity, and were used without further purification. All solvents employed in this work, including deuterated solvents, were of high purity (typically HPLC grade), and were deaerated by N₂ bubbling, followed by drying over 3 or 4 \AA molecular sieves for a minimum of 2 d before use. Acetone and acetone-*d*₆ were dried over activated CaSO₄ (DrieriteTM). THF was purchased in an inhibitor-free form and was passed through activated basic alumina to remove residual peroxides before drying. The pincer ligands AcrPNPⁱPr [11] and AcrPNPPh [5], and the Ir(I) precursors [Ir(COEt)₂Cl]₂ and [Ir(COD)Cl]₂ [64], were prepared according to previously reported procedures.

4.2. Analysis

NMR spectra were recorded using Bruker AVANCE III 300 MHz (7 T), Bruker AVANCE III 400 MHz (9.4 T) and Bruker AVANCE III HD 500 MHz (11.7 T) NMR spectrometers. All measurements were done at 25 °C, unless noted otherwise. ¹H and ¹³C NMR chemical shifts are reported in ppm relative to tetramethylsilane, and referenced to the residual protium signal of the deuterated solvent and the ¹³C signal(s) of this solvent, respectively. Assignment of the ¹H and ¹³C NMR signals was confirmed by COSY, HMBC and HSQC experiments. ¹⁵N NMR chemical shifts are reported in ppm relative to liquid ammonia, and referenced to an external sample of 90% formamide in DMSO (δ = 112.0 ppm). ¹⁹F NMR chemical shifts are reported in ppm relative to CFCl₃ and referenced to an external solution of 0.05% α,α,α -trifluorotoluene in CDCl₃ (δ = -62.7 ppm). ³¹P NMR chemical shifts are reported in ppm relative to H₃PO₄ and referenced to an external sample of 85% aqueous phosphoric acid (δ = 0.0 ppm). NMR spectra were processed and plotted with TopSpin 3.6.2 (Bruker Corp.) [65]. Abbreviations used in the description of NMR data are as follows: s, singlet; d, doublet; t, triplet; q, quartet; m, multiplet; vt, virtual triplet; Ar, aryl; br, broad peak; Acr, acridine/acridane/acridanide; \bar{J} , virtual coupling constant for which the exact identity of coupled nuclei is uncertain.

X-ray crystallographic measurements and structure elucidation were performed at the crystallographic unit of the Weizmann Institute of Science. Details pertaining to data collection and structure refinement, including a compilation of crystallographic data and refinement parameters, are available in the *Supplementary Information*. The crystallographic coordinates for the structures reported in this study have been deposited at the Cambridge Crystallographic Data Centre (CCDC) under deposition numbers 2224305–2224309, 2243893 and 2243894. Previously published crystal structures were retrieved from the CSD (v. 5.43, November 2022) [66] by using ConQuest 2022.2.0 [67], and new crystal structures were drawn and analyzed using Mercury 4.3.1 [68].

Electrospray ionization high resolution mass spectrometry (ESI-HRMS) measurements were performed at the mass spectrometry unit of the Weizmann Institute of Science, using a Waters Xevo G2-XS QToF mass spectrometer. ICP-OES measurements were carried out at the Interdepartmental Equipment Facility, Faculty of Agriculture, Food and Environment, The Hebrew University of Jerusalem, using a Spectro Arcos ICP-OES analyzer after sample predigestion with nitric acid. Infrared (IR) spectra were recorded on a Nicolet FT-IR spectrophotometer.

4.3. Synthesis of iridium complexes

4.3.1. Complex 1

98.6 mg (110 µmol) of $[\text{Ir}(\text{COE})_2\text{Cl}]_2$ were dissolved in 23 mL of THF, and the resulting solution was placed in a Schlenk flask equipped with a magnetic stirring bar. The flask was then fitted with a rubber septum and taken out of the glovebox. Ethylene gas was bubbled through the solution, with continuous stirring, for 10 min, during which its color changed from bright yellow-orange to pale yellow, indicating the *in situ* formation of $[\text{Ir}(\text{ethylene})_2\text{Cl}]_2$. The Schlenk flask was then reintroduced into the glovebox, and a solution containing 96.7 mg (220 µmol) of AcrPNPⁱPr in 3.4 mL of THF was quickly injected into the flask, leading to an immediate color change from pale yellow to dark red. The resulting mixture was stirred at room temperature for 0.5 h, after which it was placed under reduced pressure to remove volatiles, until its volume reached ~4 mL. To this concentrated solution were then added ~10 mL of pentane, with stirring, and the precipitated solids were separated by decantation, washed with $3 \times \sim 10$ mL of pentane, and placed under reduced pressure to remove residual volatiles. This afforded 135 mg (194 µmol, 88% yield) of complex 1 as red-brown solids.

¹H NMR (400 MHz, THF-d₈): 8.79 (s, 1H, C_{Acr}-H), 7.95 (d, ³J_{HH} = 8.4 Hz, 1H, C_{Acr}-H), 7.73 (d, ³J_{HH} = 6.2 Hz, 1H, C_{Acr}-H), 7.55 (d, ³J_{HH} = 6.9 Hz, 1H, C_{Acr}-H), 7.40 (d, ³J_{HH} = 8.4 Hz, 1H, C_{Acr}-H), 7.35 (t, ³J_{HH} = 7.6 Hz, 1H, C_{Acr}-H), 7.26 (t, ³J_{HH} = 7.5 Hz, 1H, C_{Acr}-H), 3.76 (m, 2H, C_{Acr}-CH₂-P), 3.05 (dd, ²J_{PH} = 5.0 Hz, ³J_{PH} = 2.3 Hz, 1H, Ir-CH-P), 2.52 (m, 3H, P-CH(CH₃)₂), 2.23 (m, 2H, Ir-CH₂CH₃), 1.98 (m, 1H, P-CH(CH₃)₂), 1.67 (dd, ³J_{HH} = 7.6 Hz, ³J_{PH} = 13.7 Hz, 3H, P-CH(CH₃)₂), 1.52 (dd, ³J_{HH} = 7.2 Hz, ³J_{PH} = 16.7 Hz, 3H, P-CH(CH₃)₂), 1.37 (m, 9H, P-CH(CH₃)₂), 1.33 (dd, ³J_{HH} = 7.3 Hz, ³J_{PH} = 10.8 Hz, 3H, P-CH(CH₃)₂) 1.12 (dd, ²J_{HH} = 7.9 Hz, ³J_{PH} = 16.5 Hz, 3H, P-CH(CH₃)₂), 0.94 (m, 6H, overlapping signals for P-CH(CH₃)₂ and Ir-CH₂CH₃). ¹³C{¹H} NMR (101 MHz, THF-d₈): 157.8 (s, C_{Acr}), 151.9 (s, C_{Acr}), 146.3 (s, C_{Acr}), 139.2 (s, C_{Acr}-H), 134.7 (s, C_{Acr}), 134.5 (d, ³J_{CP} = 6.3 Hz, C_{Acr}-H), 131.4 (vt, ³J_{CP} + ⁵J_{CP}/2 = 5.6 Hz, C_{Acr}-H), 130.7 (s, C_{Acr}), 130.0 (s, C_{Acr}-H), 127.2 (s, C_{Acr}-H), 125.5 (s, C_{Acr}-H), 122.6 (s, C_{Acr}-H), 33.9 (d, ¹J_{CP} = 24.4 Hz, C_{Acr}-CH₂-P), 25.1 (P-CH(CH₃)₂, overlapping with residual solvent peak), 24.4 (d, ¹J_{CP} = 15.8 Hz, P-CH(CH₃)₂), 24.2 (d, ¹J_{CP} = 15.8 Hz, P-CH(CH₃)₂) 23.1 (d, ²J_{CP} = 5.8 Hz, P-CH(CH₃)₂), 22.8 (d, ¹J_{CP} = 22.4 Hz, P-CH(CH₃)₂), 21.6 (d, ²J_{CP} = 5.2 Hz, P-CH(CH₃)₂), 20.9 (s, P-CH(CH₃)₂), 20.4 (s, P-CH(CH₃)₂), 19.9 (s, P-CH(CH₃)₂), 19.8 (d, ²J_{CP} = 2.5 Hz, P-CH(CH₃)₂), 19.7 (s, P-CH(CH₃)₂), 18.8 (d, ³J_{CP} = 4.2 Hz, Ir-CH₂CH₃), 17.6 (overlapping signals for Ir-CH-P and P-CH(CH₃)₂), -22.9 (Ir-CH₂CH₃). ³¹P{¹H} NMR (121 MHz, THF-d₈): 10.2 (d, ²J_{PP} = 19.5 Hz, CH₂-P-Ir), -30.0 (d, ²J_{PP} = 19.5 Hz, CH-P-Ir). ESI-HRMS (MeOH): M⁺, m/z 632.2198; calcd. for C₂₇H₃₉IrNP₂ (complex - Cl⁻ - ethylene), 632.2187.

4.3.2. Complex 2

Complex 2 was synthesized using the same procedure as for complex 1, but replacing ligand AcrPNPⁱPr with AcrPNPPh. Using 100 mg (112 µmol) of $[\text{Ir}(\text{COE})_2\text{Cl}]_2$ afforded 180 mg (217 µmol, 97% yield) of complex 2 as red solids. This compound is practically insoluble in most conventional solvents, but is soluble in dichloromethane. It is unstable in this solvent at room temperature, and was characterized at -10 °C.

¹H NMR (500 MHz, CD₂Cl₂, -10 °C): 9.11 (s, 1H, C_{Acr}-H), 8.12 (d, ³J_{HH} = 8.4 Hz, 1H, Ar-H), 8.05 (d, ³J_{HH} = 8.3 Hz, 1H, Ar-H), 7.95 (m, 2H, Ar-H), 7.82 (d, ³J_{HH} = 6.8 Hz, 1H, Ar-H), 7.64 (d, ³J_{HH} = 6.5 Hz, 1H, Ar-H), 7.58–7.49 (m, 4H, Ar-H), 7.40 (br, 3H, Ar-H), 7.36 (m, 1H, Ar-H), 7.28 (m, 3H, Ar-H), 7.10–7.01 (m, 7H, Ar-H), 6.89 (t, ³J_{HH} = 7.1 Hz, 2H, Ar-H), 4.65 (dd, ²J_{PH} = 10.6, ²J_{HH} = 15.1 Hz, 1H, C_{Acr}-CH₂-P), 4.12 (m, 2H, C_{Acr}-CH₂-P), 3.56 (t, ²J_{HH} ≈ ²J_{PH} ≈ 12.8 Hz, 1H, C_{Acr}-CH₂-P), 2.56 (t, J_{HH} = 9.3 Hz, 1H, Ir(C₂H₄)), 2.49 (m, 1H, Ir(C₂H₄)), 0.61 (m, 1H, Ir(C₂H₄)), -0.05 (m, 1H, Ir(C₂H₄)). ¹³C{¹H} NMR (126 MHz, CD₂Cl₂, -10 °C): 152.3 (s, C_{Ar}), 151.8 (s, C_{Ar}), 139.9 (s, C_{Ar}), 138.5 (s, C_{Ar}), 138.2 (s, C_{Ar}), 135.7 (s, C_{Ar}), 135.6 (s, C_{Ar}), 134.9 (s, C_{Ar}), 134.2–131.8 (overlapping signals of C_{Ar}), 129.9–126.9 (overlapping

signals of C_{Ar}), 125.7 (s, C_{Ar}), 125.2 (s, C_{Ar}), 34.8 (d, ¹J_{CP} = 24.3 Hz, C_{Acr}-CH₂-P), 32.5 (d, ¹J_{CP} = 36.5 Hz, C_{Acr}-CH₂-P), 26.9 (d, ²J_{CP} = 41.0 Hz, Ir(C₂H₄)), 26.3 (s, Ir(C₂H₄)). ³¹P{¹H} NMR (202 MHz, CD₂Cl₂, -10 °C): 24.6 (d, ²J_{PP} = 17.4 Hz), 11.5 (d, ²J_{PP} = 17.4 Hz). ESI-HRMS (MeOH): M⁺, m/z 796.1868; calcd. for C₄₁H₃₅IrNP₂ (complex - Cl⁻), 796.1874.

4.3.3. Complex 3

40.6 mg (58.4 µmol) of complex 1 were dissolved in 4.5 mL of THF, and the resulting solution was loaded into a Fischer-Porter pressure tube, which was then pressurized with 2 bar of H₂. The tube containing the reaction mixture was immersed in an oil bath at 80 °C, and the mixture was stirred for 1 h under these conditions. The reactor was then cooled to room temperature, and returned into the glovebox after venting off the excess gas. ~10 mL of pentane were added to the reaction mixture, with stirring, and the precipitated solids were separated by decantation, washed with 3 × ~2 mL of pentane, and placed under reduced pressure to remove residual volatiles. This gave 24.6 mg (36.8 µmol, 63% yield) of complex 3 as brown solids.

¹H NMR (500 MHz, C₆D₆): 8.33 (s, 1H, C_{Acr}-H), 7.61 (d, ³J_{HH} = 8.4 Hz, 2H, C_{Acr}-H), 7.42 (d, ³J_{HH} = 6.7 Hz, 2H, C_{Acr}-H), 7.10 (t, ³J_{HH} = 7.5 Hz, 3H, C_{Acr}-H), 3.91 (d, ²J_{HH} = 11.9 Hz, 2H, C_{Acr}-CH₂-P), 3.27 (d, ²J_{HH} = 12.4 Hz, 2H, C_{Acr}-CH₂-P), 2.09 (m, 2H, P-CH(CH₃)₂), 1.91 (m, 2H, P-CH(CH₃)₂), 1.38 (dd, ³J_{PH} = 18.3 Hz, ³J_{HH} = 7.7 Hz, 6H, P-CH(CH₃)₂), 1.24 (m, 6H, P-CH(CH₃)₂), 1.17 (dd, ³J_{PH} = 15.8 Hz, ³J_{HH} = 7.1 Hz, 6H, P-CH(CH₃)₂), 1.08 (dd, ³J_{PH} = 13.3 Hz, ³J_{HH} = 6.0 Hz, 6H, P-CH(CH₃)₂), -23.21 (td, ²J_{PH} = 18.1 Hz, ²J_{HH} = 7.8 Hz, 1H, Ir-H), -28.64 (td, ²J_{PH} = 15.7 Hz, ²J_{HH} = 7.9 Hz, 1H, Ir-H). ¹³C{¹H} NMR (126 MHz, C₆D₆): 151.9 (s, C_{Acr}), 142.8 (s, C_{Acr}-H), 133.7 (s, C_{Acr}), 133.3 (vt, (³J_{CP} + ⁵J_{CP})/2 = 3.5 Hz, C_{Acr}-H), 129.1 (s, C_{Acr}-H), 128.7 (s, C_{Acr}), 128.0 (s, C_{Acr}-H), 123.9 (s, C_{Acr}-H), 32.5 (vt, (¹J_{CP} + ³J_{CP})/2 = 10.2 Hz, C_{Acr}-CH₂-P), 22.8 (vt, (²J_{CP} + ⁴J_{CP})/2 = 17.9 Hz, P-CH(CH₃)₂), 21.1 (vt, (¹J_{CP} + ³J_{CP})/2 = 11.5 Hz, P-CH(CH₃)₂), 19.7 (vt, (²J_{CP} + ⁴J_{CP})/2 = 2.9 Hz, P-CH(CH₃)₂), 18.7 (s, P-CH(CH₃)₂), 16.5 (s, P-CH(CH₃)₂). ³¹P{¹H} NMR (121 MHz, C₆D₆): 55.5 (s). ESI-HRMS (MeOH): M⁺, m/z 632.2198; calcd. for C₂₇H₃₉IrNP₂ (complex - Cl⁻ - H₂), 632.2187.

4.3.4. Complex 4

91.1 mg (110 µmol) of complex 2 were suspended in 4.5 mL of THF, and the mixture was placed in a Fischer-Porter pressure tube, which was then pressurized with 2 bar of H₂. The reaction mixture was stirred at room temperature for 1 h, after which the excess gas was released, and the reactor was returned into the glovebox. The product was then precipitated by adding ~10 mL of pentane to the stirring reaction mixture. The solids were separated by decantation, washed with 3 × ~2 mL of pentane, and placed under reduced pressure to remove residual volatiles. This afforded 83.6 mg (104 µmol, 95% yield) of complex 4 as orange solids.

¹H NMR (400 MHz, CDCl₃): 9.11 (s, 1H, C_{Acr}-H), 8.08 (d, ³J_{HH} = 8.2 Hz, 2H, C_{Acr}-H), 7.85–7.77 (m, 8H, overlapping signals for Ar-H), 7.43–7.25 (m, 20H, overlapping signals for Ar-H and residual solvent peak), 4.51 (m, 4H, C_{Acr}-CH₂-P), -22.90 (td, ²J_{HH} = 6.8, ²J_{PH} = 22.4 Hz, 1H, Ir-H), -26.46 (td, ²J_{HH} = 6.8, ²J_{PH} = 16.9 Hz, 1H, Ir-H). ¹³C{¹H} NMR (101 MHz, CDCl₃): 153.2 (s, C_{Ar}), 143.1 (s, C_{Ar}-H), 135.9 (vt, ¹J_{CP} = 4.2 Hz, C_{Ar}-H), 135.0 (vt, ¹J_{CP} = 6.6 Hz, C_{Ar}-H), 135.0 (vt, ¹J_{CP} = 6.6 Hz, C_{Ar}), 132.2 (vt, ¹J_{CP} = 5.7 Hz, C_{Ar}), 132.0 (s, C_{Ar}), 129.9 (s, C_{Ar}-H), 129.5–129.4 (m, overlapping signals for C_{Ar}-H), 128.6 (s, C_{Ar}-H), 128.0 (vt, ¹J_{CP} = 5.0 Hz, C_{Ar}-H), 127.8 (vt, ¹J_{CP} = 5.1 Hz, C_{Ar}-H), 124.9 (m, C_{Ar}-H), 36.3 (vt, (¹J_{CP} + ³J_{CP})/2 = 13.2 Hz, C_{Acr}-CH₂-P). ³¹P{¹H} NMR (162 MHz, CDCl₃): 23.1 (s). ESI-HRMS (MeOH): M⁺, m/z 768.1577; calcd. for C₃₉H₃₁IrNP₂ (complex - Cl⁻ - H₂), 768.1561.

4.3.5. Complex 5

18.0 mg (26.9 µmol) of complex 3 were suspended in 0.34 mL of

THF-d₈ and the mixture was placed in an NMR tube, which was then fitted with a rubber septum. Separately, a solution was prepared by mixing 27.1 μ L of 1.0 M NaBEt₃H (26.9 μ mol) in toluene with 0.34 mL of THF-d₈. The hydride solution was loaded into a syringe fitted with a needle, which was then capped with a rubber plug. Both the NMR tube and syringe were taken out of the glovebox. The solution containing complex 3 was cooled to -15°C by dipping the NMR tube in a water-ice/acetone bath, and the hydride solution was then injected into the tube, which was quickly shaken manually to ensure thorough mixing. The reaction mixture was then warmed to ambient temperature and monitored by ³¹P NMR spectroscopy to ensure full conversion of 3 into 5 as the only observable product, which required ~ 15 min at this temperature. During this time, red solids were observed to settle at the bottom of the NMR tube. This NMR tube was subsequently loaded into the NMR spectrometer, which was precooled to -20°C , and the reaction product, complex 5, was characterized *in situ* at this low temperature.

¹H NMR (400 MHz, THF-d₈, -20°C): 6.74 (d, ³J_{HH} = 7.3 Hz, 2H, C_{Acr}-H), 6.64 (d, ³J_{HH} = 7.3 Hz, 2H, C_{Acr}-H), 6.28 (t, ³J_{HH} = 7.3 Hz, 2H, C_{Acr}-H), 3.89 (d, ²J_{HH} = 16.5 Hz, 1H, C_{Acr}-CH₂-C_{Acr}), 3.64 (d, ²J_{HH} = 16.5 Hz, 1H, C_{Acr}-CH₂-C_{Acr}, overlapping with residual solvent peak), 3.33 (m, 2H, C_{Acr}-CH₂-P), 2.46 (m, 2H, C_{Acr}-CH₂-P, overlapping with Ar-CH₃ of toluene), 2.26 (m, 2H, P-CH(CH₃)₂, overlapping with Ar-CH₃ of toluene), 1.56 (m, 2H, P-CH(CH₃)₂), 1.39–1.30 (m, 12H, P-CH(CH₃)₂, overlapping with residual pentane), 1.18 (dd, ³J_{PH} = 12.4 Hz, ³J_{HH} = 7.1 Hz, 6H, P-CH(CH₃)₂), 1.06 (dd, ³J_{PH} = 13.7 Hz, ³J_{HH} = 7.4 Hz, 6H, P-CH(CH₃)₂), -13.03 (m, 2H, *trans* Ir(H)₂), -23.56 (m, 1H, Ir-H). ¹³C{¹H} NMR (101 MHz, THF-d₈, -20°C): 160.2 (s, C_{Acr}), 128.2 (m, C_{Acr}-H), 126.9 (s, C_{Acr}), 124.8 (s, C_{Acr}), 124.6 (s, C_{Acr}-H), 115.0 (s, C_{Acr}-H), 35.6 (s, C_{Acr}-CH₂-C_{Acr}), 30.9 (d, ¹J_{CP} = 33.8 Hz, P-CH(CH₃)₂), 26.4 (m, overlapping signals for C_{Acr}-CH₂-P and P-CH(CH₃)₂), 21.9 (bs, P-CH(CH₃)₂), 21.6 (s, P-CH(CH₃)₂), 21.3 (s, P-CH(CH₃)₂) 19.2 (s, P-CH(CH₃)₂). ³¹P{¹H} NMR (162 MHz, THF-d₈, -20°C): 62.2 (s).

³¹P{¹H} NMR (162 MHz, THF-d₈): 62.2 (s). ²³Na NMR (106 MHz, THF), after addition of 2 equiv of 18-crown-6: -9.77 (br).

4.3.6. Complex 6

A THF solution of NaBEt₃H was prepared by adding 45.2 μ L of 1.0 M NaBEt₃H (44.8 μ mol) in toluene to 3.4 mL of THF. The resulting solution was added dropwise to a stirring solution comprising 30.0 mg (44.8 μ mol) of complex 3 in 3.4 mL of THF. The reaction mixture was then stirred at room temperature for 30 min, and the volatiles were subsequently removed under reduced pressure. The remaining solid residue was extracted with 7 mL of benzene, and the afforded solution was filtered through a plug of celite and frozen at -35°C . The frozen extract was placed under high vacuum to remove the solvent, thereby affording 22.4 mg (35.3 μ mol, 79% yield) of complex 6 as a microcrystalline orange powder.

¹H NMR (400 MHz, THF-d₈, -30°C): 7.09 (d, ³J_{HH} = 6.7 Hz, 2H, C_{Acr}-H), 7.01 (d, ³J_{HH} = 7.3 Hz, 2H, C_{Acr}-H), 6.71 (t, ³J_{HH} = 7.3 Hz, 2H, C_{Acr}-H), 3.72 (d, ²J_{HH} = 14.7 Hz, 1H, overlapping signals for C_{Acr}-CH₂-C_{Acr} and residual solvent peak), 3.58 (d, ²J_{HH} = 14.7 Hz, 1H, C_{Acr}-CH₂-C_{Acr}), 3.37 (br, 4H, C_{Acr}-CH₂-P), 2.34 (br, 2H, P-CH(CH₃)₂), 1.63 (br, 2H, P-CH(CH₃)₂), 1.33 (dd, ²J_{PH} = 16.7 Hz, ²J_{HH} = 6.9 Hz, 6H, P-CH(CH₃)₂), 1.24 (m, 18H, P-CH(CH₃)₂), -26.92 (br, 1H, Ir-H), -27.57 (br, 1H, Ir-H). ¹³C{¹H} NMR (101 MHz, THF-d₈, -30°C): 152.5 (m, C_{Acr}) 128.3 (m, C_{Acr}-H), 127.4 (s, C_{Acr}) 125.6 (s, C_{Acr}-H), 122.1 (s, C_{Acr}), 118.1 (s, C_{Acr}-H), 35.6 (s, C_{Acr}-CH₂-C_{Acr}), 27.2 (m, C_{Acr}-CH₂-P), 23.9 (m, P-CH(CH₃)₂, overlapping with solvent peak), 23.6 (vt, ¹J_{CP} + ³J_{CP}/2 = 11.8 Hz, P-CH(CH₃)₂), 20.4 (br, P-CH(CH₃)₂), 18.4 (s, P-CH(CH₃)₂), 18.0 (s, P-CH(CH₃)₂). ³¹P{¹H} NMR (162 MHz, THF-d₈, -30°C): 67.0 (br).

¹H NMR (300 MHz, THF-d₈): 7.05 (d, ³J_{HH} = 7.1 Hz, 2H, C_{Acr}-H), 6.93 (d, ³J_{HH} = 7.2 Hz, 2H, C_{Acr}-H), 6.66 (t, ³J_{HH} = 7.3 Hz, 2H, C_{Acr}-H), 3.65 (d, ²J_{HH} = 14.3 Hz, 2H, overlapping signals for C_{Acr}-CH₂-C_{Acr} and residual solvent peak), 3.49 (d, ²J_{HH} = 14.1 Hz, 1H, C_{Acr}-CH₂-C_{Acr}), 3.27 (m, 4H, C_{Acr}-CH₂-P), 2.24 (m, 2H, P-CH(CH₃)₂), 1.53 (m, 2H,

P-CH(CH₃)₂), 1.31 (dd, ²J_{PH} = 16.3 Hz, ²J_{HH} = 6.7 Hz, 6H, P-CH(CH₃)₂), 1.18 (dd, ²J_{PH} = 15.5 Hz, ²J_{HH} = 7.4 Hz, 9H, P-CH(CH₃)₂), 1.11 (dd, ²J_{PH} = 14.4 Hz, ²J_{HH} = 6.9 Hz, 9H, P-CH(CH₃)₂), -26.89 (br, 1H, Ir-H), -28.18 (br, 1H, Ir-H). ³¹P{¹H} NMR (162 MHz, THF-d₈): 68.6 (br). ESI-HRMS (MeOH): M⁺, *m/z* 632.2195; calcd. for C₂₇H₃₉IrNP₂ (complex - H⁺ - H₂), 632.2187.

4.3.7. Complex 7

To a solution of 5.0 mg (3.20 μ mol) of complex 6 in 0.6 mL of C₆D₆ were added \sim 10 mg (\sim 13 μ mol) of CD₃CN, and the mixture was shaken manually. Complex 7 was the only observable product in solution and was characterized *in situ*.

¹H NMR (400 MHz, C₆D₆): 7.23 (d, ³J_{HH} = 7.0 Hz, 2H, C_{Acr}-H), 7.01 (d, ³J_{HH} = 7.0 Hz, 2H, C_{Acr}-H), 6.88 (t, ³J_{HH} = 7.2 Hz, 2H, C_{Acr}-H), 3.96 (d, ²J_{HH} = 15.1 Hz, 1H, C_{Acr}-CH₂-C_{Acr}), 3.81 (d, ²J_{HH} = 15.1 Hz, 1H, C_{Acr}-CH₂-C_{Acr}), 3.15 (m, 2H, C_{Acr}-CH₂-P, overlapping with residual solvent peak), 3.15 (m, 2H, C_{Acr}-CH₂-P), 1.96 (m, 2H, P-CH(CH₃)₂), 1.56 (m, 2H, P-CH(CH₃)₂), 1.21 (dd, ²J_{PH} = 16.8 Hz, ²J_{HH} = 7.4 Hz, 6H, P-CH(CH₃)₂), 1.09 (m, 18H, P-CH(CH₃)₂), -22.43 (td, ²J_{HH} = 6.9, ²J_{PH} = 15.7 Hz, 1H, Ir-H), -22.90 (td, ²J_{HH} = 6.9, ²J_{PH} = 19.1 Hz, 1H, Ir-H). ¹³C{¹H} NMR (101 MHz, C₆D₆): 151.0 (s, C_{Acr}), 128.6 (vt, ¹J_{CP} = 2.6 Hz, C_{Acr}-H), 126.0 (s, C_{Acr}-H), 125.7 (s, C_{Acr}), 121.7 (s, C_{Acr}), 116.0 (s, C_{Acr}-H), 36.9 (s, C_{Acr}-CH₂-C_{Acr}), 33.1 (vt, ¹J_{CP} + ³J_{CP}/2 = 13.3 Hz, C_{Acr}-CH₂-P), 23.7 (vt, ¹J_{CP} + ³J_{CP}/2 = 17.4 Hz, P-CH(CH₃)₂), 22.6 (vt, ¹J_{CP} + ³J_{CP}/2 = 11.2 Hz, P-CH(CH₃)₂), 22.2 (m, P-CH(CH₃)₂), 19.3 (vt, ²J_{CP} + ⁴J_{CP}/2 = 3.0 Hz, P-CH(CH₃)₂), 18.9 (s, P-CH(CH₃)₂) 16.4 (s, P-CH(CH₃)₂). ³¹P{¹H} NMR (162 MHz, C₆D₆): 60.3 (s).

4.3.8. Complex 8

Complex 8 was isolated as orange crystals from a THF solution of complex 6 that was kept in an open vessel inside the glovebox, thereby allowing slow solvent evaporation at room temperature. One of these crystals was subjected to X-ray crystallographic analysis, and the resulting crystal structure is presented in the [Supplementary Information](#).

Crystals of 8 were also isolated from two other samples: (a) Crude reaction mixture obtained from complex 3 and NaBEt₃H in THF (see procedure for the synthesis of complex 5), which was overlaid with pentane and kept at -35°C ; (b) The same type of crude reaction mixture in THF-d₈, placed in an open vial in the glovebox and allowed to slowly evaporate at room temperature. In both cases, the identity of 8 was confirmed by X-ray crystallographic analysis.

4.3.9. Complex 9

A THF solution of NaBEt₃H was prepared by mixing 25.0 μ L of 1.0 M NaBEt₃H (24.8 μ mol) in toluene with 1.4 mL of THF. The afforded solution was added dropwise to a stirring suspension comprising 20.0 mg (24.8 μ mol) of complex 4 in 1.4 mL of THF. The reaction mixture was then stirred at room temperature for 2 min, during which it changed from an orange suspension into a clear orange solution. 11 mL of pentane were then added to this reaction mixture, causing orange solids to precipitate. The pale yellow supernatant was decanted, and the solids were extracted with 2×3 mL of pentane. The liquid fractions were then combined and the solvent was pumped off to give 8.8 mg (11.1 μ mol, 45% yield) of complex 9 as a yellow semisolid. This complex is unstable in solution at room temperature, and was characterized at -20°C .

¹H NMR (400 MHz, THF-d₈, -20°C): 7.92 (m, 4H, Ar-H), 7.28–7.19 (m, 10H, overlapping signals for Ar-H), 6.99 (t, *J* = 7.3 Hz, 2H, Ar-H), 6.84 (m, *J* = 7.3 Hz, 4H, Ar-H), 6.73 (d, ³J_{HH} = 7.3 Hz, 4H, C_{Acr}-H), 6.31 (t, ³J_{HH} = 7.3 Hz, 2H, C_{Acr}-H), 4.08 (m, 3H, overlapping signals for C_{Acr}-CH₂-C_{Acr} and C_{Acr}-CH₂-P), 3.80 (d, ²J_{HH} = 16.9 Hz, 1H, C_{Acr}-CH₂-C_{Acr}), 3.32 (dd, ²J_{PH} = 11.8 Hz, ²J_{HH} = 6.5 Hz, 2H, C_{Acr}-CH₂-P), -11.75 (m, 2H, *trans* Ir(H)₂), -21.92 (m, 1H, Ir-H). ¹³C{¹H} NMR (101 MHz, THF-d₈, -20°C): 160.0 (s, C_{Acr}), 141.7 (d, ¹J_{CP} = 47.9 Hz, C_{Ar}-P-CH₂-Acr), 137.3 (d, ¹J_{CP} = 47.9 Hz, C_{Ar}-P-CH₂-Acr),

134.5 (vt, $J_{CP} = 5.8$ Hz, C_{Ar-H}), 130.9 (vt, $J_{CP} = 5.0$ Hz, C_{Ar-H}), 127.7 (m, C_{Acr-H}), 127.1 (s, C_{Ar-H}), 127.0 (vt, $J_{CP} = 3.9$ Hz, C_{Ar-H}), 126.5 (vt, $J_{CP} = 4.2$ Hz, C_{Ar-H}), 124.7 (s, C_{Acr}), 124.0 (s, C_{Acr-H}), 123.9 (s, C_{Acr}), 114.6 (s, C_{Acr-H}), 34.2 (s, $C_{Acr}-CH_2-C_{Acr}$), 32.0 (d, $J_{CP} = 22.9$ Hz, $C_{Acr}-CH_2-P$). $^{31}P\{^1H\}$ NMR (162 MHz, THF-d₈, -20 °C): 49.4 (s).

$^{31}P\{^1H\}$ NMR (162 MHz, THF-d₈): 48.8 (s). ^{23}Na NMR (79 MHz, THF): 12.3 (br). ^{23}Na NMR (79 MHz, THF), after addition of 0.6 equiv of 18-crown-6: -6.1 (br).

4.3.10. Complex 10

A THF solution of NaBET₃H was prepared by adding 14.4 µl of 1.0 M NaBET₃H (14.3 µmol) in toluene to 0.3 mL of THF. The resulting solution was added dropwise to a stirring suspension comprising 11.5 mg (14.3 µmol) of complex 4 in 0.3 mL of THF. The reaction mixture was then stirred at room temperature for 30 min, and the volatiles were subsequently removed under reduced pressure. The remaining solid residue was extracted with 7 mL of benzene, and the resulting solution was filtered through a plug of celite and frozen at -35 °C. The frozen extract was placed under high vacuum to remove the solvent, thereby affording 6.5 mg (4.22 µmol, 60% yield) of complex 10 as a microcrystalline yellow-green powder.

1H NMR (400 MHz, C₆D₆): 7.29 (m, 12H, Ar-H), 7.11 (m, 8H, Ar-H), 6.90 (t, $^3J_{HH} = 7.3$ Hz, 4H, Ar-H), 6.82 (m, 8H, Ar-H), 6.70 (m, 12H, Ar-H), 6.54 (t, $^3J_{HH} = 7.6$ Hz, 8H, Ar-H), 5.30 (d, $^2J_{HH} = 15.4$ Hz, 2H, C_{Acr}-CH₂-C_{Acr}), 4.20 (d, $^2J_{HH} = 15.6$ Hz, 2H, C_{Acr}-CH₂-C_{Acr}), 3.24 (m, 4H, C_{Acr}-CH₂-P), 2.41 (m, 4H, C_{Acr}-CH₂-P), -7.98 (tt, $^2J_{PH} = 66.5$ Hz, $^2J_{HH} = 3.6$ Hz, 2H, Ir-H-Ir), -13.94 (m, 2H, Ir-H). $^{13}C\{^1H\}$ NMR (101 MHz, C₆D₆): 156.0 (s, C_{Ar}), 133.2 (br, C_{Ar-H}), 129.6 (s, C_{Ar}), 129.5 (s, C_{Ar-H}), 129.1 (s, C_{Ar-H}), 128.1 (m, C_{Ar-H}), 128.0 (C_{Ar}, overlapping with residual solvent peak), 127.5 (C_{Ar-H}, overlapping with residual solvent peak), 126.2 (s, C_{Ar-H}), 122.6 (s, C_{Ar}), 117.5 (s, C_{Ar-H}), 37.3 (s, C_{Acr}-CH₂-C_{Acr}), 34.9 (vt, $^1J_{CP} + ^3J_{CP}/2 = 16.4$ Hz, C_{Acr}-CH₂-P). $^{31}P\{^1H\}$ NMR (162 MHz, C₆D₆): 20.1 (s). ESI-HRMS (MeOH): M⁺, m/z 1541.3589; calcd. for C₇₈H₆₇Ir₂N₂P₄ (complex - H⁻), 1541.3513.

4.3.11. Complex 11

A solution of 5.1 mg (26 µmol) of AgBF₄ in 0.40 mL of acetone was added dropwise to a stirring suspension comprising 11.6 mg (13 µmol) of [Ir(COF)₂Cl]₂ in 0.15 mL of acetone, and the resulting mixture was stirred in the dark, at room temperature, for 20 min. It was then filtered through a bed of celite, which was subsequently washed with 0.4 mL of acetone. The filtrates were combined and added dropwise into a stirred suspension of 14.9 mg (26 µmol) of AcrPNPPh in 0.14 mL of acetone. The afforded orange solution was stirred at room temperature for 20 min, after which 9 mL of pentane were added to this stirring solution, causing the precipitation of yellow solids. The supernatant was decanted, and the solids were washed with 2 × 5 mL of pentane and then placed under reduced pressure to remove residual volatiles. This gave 17.6 mg (18.2 µmol, 70% yield) of complex 11 as a yellow powder.

1H NMR (400 MHz, acetone-d₆): 9.70 (s, 1H, C_{Acr-H}), 8.61 (d, $^3J_{HH} = 7.0$ Hz, 2H, C_{Acr-H}), 8.44 (d, $^3J_{HH} = 8.4$ Hz, 2H, C_{Acr-H}), 7.98 (m, 4H, Ar-H), 7.88 (t, $^3J_{HH} = 7.5$ Hz, 2H, C_{Acr-H}), 7.56–7.42 (m, 10H, Ar-H), 7.14 (m, 2H, Ar-H), 7.02 (m, 4H, Ar-H), 5.18 (t, $^2J_{PH} \approx ^2J_{HH} \approx 14.3$ Hz, 2H, C_{Acr}-CH₂-P), 3.96 (dd, $^2J_{PH} \approx ^2J_{HH} \approx 12.7$ Hz, 2H, C_{Acr}-CH₂-P), 2.42 (m, 2H, η^3 -cyclooctenyl: Ir(CHCHCH)), 1.15–1.03 (m, 2H, η^3 -cyclooctenyl: CH(CH₂)₅CH), 0.89–0.72 (m, 4H, η^3 -cyclooctenyl: CH(CH₂)₅CH), 0.65–0.55 (m, 2H, η^3 -cyclooctenyl: CH(CH₂)₅CH), 0.50–0.42 (m, 2H, η^3 -cyclooctenyl: CH(CH₂)₅CH), -0.05 (t, $^3J_{HH} = 8.2$ Hz, 1H, η^3 -cyclooctenyl: Ir(CHCHCH)), -27.50 (t, $^2J_{PH} = 15.6$ Hz, 1H, Ir-H). $^{13}C\{^1H\}$ NMR (101 MHz, acetone-d₆): 154.8 (s, C_{Acr}), 145.8 (s, C_{Acr-H}), 137.8 (d, $^3J_{CP} = 9.0$ Hz, C_{Acr-H}), 137.2 (dd, $^1J_{CP} = 55.1$ Hz, $^3J_{CP} = 2.0$ Hz, C_{Ar}), 134.3 (d, $^2J_{CP} = 3.1$ Hz, C_{Acr}), 132.7 (d, $J_{CP} = 10.2$ Hz, C_{Ar-H}), 132.2 (d, $^1J_{CP} = 49.1$ Hz, C_{Ar}, overlapping with the next doublet), 132.1 (d, $J_{CP} = 9.8$ Hz, C_{Ar-H}), 131.1 (d, $J_{CP} = 2.5$ Hz, C_{Ar-H}), 130.9 (d, $J_{CP} = 2.4$ Hz, C_{Ar-H}), 129.7 (d, $J_{CP} = 3.3$ Hz, C_{Acr-H}), 129.5 (d,

J_{CP} = 10.5 Hz, C_{Ar-H}), 129.2 (s, C_{Acr}, overlapping with the next doublet), 129.1 (d, J_{CP} = 10.4 Hz, C_{Ar-H}), 127.8 (d, J_{CP} = 2.6 Hz, C_{Acr-H}), 104.7 (s, η^3 -cyclooctenyl: Ir(CHCHCH)), 62.4 (d, $^2J_{CP} = 29.1$ Hz, η^3 -cyclooctenyl: Ir(CHCHCH)), 35.0 (d, J_{CP} = 3.1 Hz, η^3 -cyclooctenyl: CH(CH₂)₅CH), 31.9 (d, $^1J_{CP} = 30.2$ Hz, C_{Acr}-CH₂-P), 28.5 (d, J_{CP} = 6.0 Hz, η^3 -cyclooctenyl: CH(CH₂)₅CH), 24.94 (s, η^3 -cyclooctenyl: CH(CH₂)₅CH). $^{31}P\{^1H\}$ NMR (121 MHz, acetone-d₆): 21.3 (s). $^{19}F\{^1H\}$ NMR (282 MHz, acetone-d₆): -151.6 (s). ESI-HRMS (MeOH): M⁺, m/z 878.2686; calcd. For C₄₇H₄₅IrNP₂ (complex - BF₄⁻), 878.2656.

4.3.12. Complex 12

A solution of 30.0 mg (31.1 µmol) of complex 11 in 3.8 mL of acetone was loaded into a Fischer-Porter pressure tube. The headspace was pumped off until solvent boiling was visible, and it was then pressurized with 2 bar of H₂. The reactor was dipped in an oil bath at 50 °C, and the solution was stirred at this temperature for 24 h. The excess gas was then vented off, and the pressure tube was returned into the glovebox. The product was precipitated by adding ~10 mL of pentane to the stirring reaction mixture, and the supernatant was decanted. The resulting solids were washed with 2 × ~5 mL of pentane and placed under reduced pressure to remove residual volatiles. This afforded 26.6 mg (27.5 µmol, 88% yield) of complex 12 as a yellow powder.

1H NMR (400 MHz, acetone-d₆): 7.81 (d, $^3J_{HH} = 7.2$ Hz, 2H, Ar-H), 7.72 (m, 4H, Ar-H), 7.51–7.32 (m, 14H, Ar-H), 7.14 (t, $^3J_{HH} = 7.3$ Hz, 3H, Ar-H), 7.00 (m, 3H, Ar-H), 5.04 (t, $^2J_{PH} \approx ^2J_{HH} \approx 15.0$ Hz, 2H, C_{Acr}-CH₂-P), 4.80 (d, $^2J_{HH} = 21.7$ Hz, 1H, C_{Acr}-CH₂-C_{Acr}), 4.52 (d, $^2J_{HH} = 21.7$ Hz, 1H, C_{Acr}-CH₂-C_{Acr}), 3.87 (m, 3H, overlapping signals for C_{Acr}-CH₂-P and η^3 -cyclooctenyl: Ir(CHCHCH)), 2.74 (m, 2H, η^3 -cyclooctenyl: Ir(CHCHCH)), 1.29 (m, 4H, η^3 -cyclooctenyl: CH(CH₂)₅CH), 0.87 (br, 4H, η^3 -cyclooctenyl: CH(CH₂)₅CH), 0.46 (br, 2H, η^3 -cyclooctenyl: CH(CH₂)₅CH), -25.74 (t, $^2J_{PH} = 15.9$ Hz, 1H, Ir-H). $^{13}C\{^1H\}$ NMR (126 MHz, acetone-d₆): 138.3 (s, C_{Ar}), 137.4 (s, C_{Ar}), 137.0 (s, C_{Ar}), 132.9 (d, $J_{CP} = 10.5$ Hz, C_{Ar-H}), 131.8 (m, overlapping signals for C_{Ar-H}), 131.5 (s, C_{Ar}), 131.2 (s, C_{Ar-H}), 130.9 (s, C_{Ar-H}), 129.4 (m, overlapping signals for C_{Ar-H}), 129.1 (d, $J_{CP} = 10.7$ Hz, C_{Ar-H}), 127.7 (s, C_{Ar}), 127.0 (s, C_{Ar-H}), 125.2 (s, C_{Ar}), 105.0 (s, η^3 -cyclooctenyl: Ir(CHCHCH)), 64.2 (d, $^2J_{CP} = 29.7$ Hz, η^3 -cyclooctenyl: Ir(CHCHCH)), 34.2 (s, η^3 -cyclooctenyl: CH(CH₂)₅CH), 31.8 (d, $^1J_{CP} = 27.1$ Hz, C_{Acr}-CH₂-P), 30.3 (s, C_{Acr}-CH₂-C_{Acr}, overlapping with solvent residual peak), 28.6 (s, η^3 -cyclooctenyl: CH(CH₂)₅CH). $^{31}P\{^1H\}$ NMR (162 MHz, acetone-d₆): 23.7 (s). $^{19}F\{^1H\}$ NMR (282 MHz, acetone): -153.0 (s). IR (KBr; cm⁻¹): 3255 (w, ν_{N-H}), 3051 (w), 2918 (w), 2225 (w), 1657 (w), 1435 (s), 1093 (vs, ν_{B-P}). ESI-HRMS (MeOH): M⁺, m/z 878.2692; calcd. for C₄₇H₄₇IrNP₂ (complex - H₂ - BF₄⁻), 878.2656.

4.3.13. Complex 13

A solution of 29.0 mg (149 µmol) of AgBF₄ in 2.2 mL of acetone was added dropwise to a stirring suspension of 50.1 mg (74 µmol) of [Ir(COD)Cl]₂ in 0.84 mL of acetone, and the resulting mixture was stirred in the dark, at room temperature, for about 20 min. It was then filtered through a bed of celite, which was subsequently washed with ~0.5 mL of acetone. The filtrates were combined and added dropwise to a stirring suspension of 85.7 mg (149 µmol) of AcrPNPPh in 0.90 mL of acetone. The resulting red solution was stirred at room temperature for ~20 min, after which 15 mL of pentane were added to this stirring solution, causing the precipitation of red solids. The supernatant was decanted, and the solids were washed with 2 × 5 mL of pentane and then placed under reduced pressure to remove residual volatiles. This gave 132.9 mg (138 µmol, 93% yield) of complex 13 as a red powder.

1H NMR (500 MHz, acetone-d₆): 9.66 (s, 1H, C_{Acr-H}), 8.45 (d, $^3J_{HH} = 8.4$ Hz, 2H, C_{Acr-H}), 8.00 (d, $^3J_{HH} = 6.8$ Hz, 2H, C_{Acr-H}), 7.79 (t, $^3J_{HH} = 7.6$ Hz, 2H, C_{Acr-H}), 7.38 (m, 20H, Ar-H), 4.38 (br, 2H, C_{Acr}-CH₂-P), 3.84 (br, 2H, C_{Acr}-CH₂-P), 3.46 (s, 4H, η^2,η^2 -COD: Ir(CH = CH)₂), 1.44–1.29 (m, 8H, η^2,η^2 -COD: CH(CH₂)₄CH). $^{13}C\{^1H\}$ NMR (126 MHz, acetone-d₆): 150.4 (s, C_{Ar}), 142.0 (s, C_{Acr-H}), 136.3 (t, $^3J_{CP} + ^5J_{CP}/2 = 4.6$ Hz, C_{Acr-H}), 135.4 (br, C_{Ar-H}), 134.0 (br, C_{Ar-H}), 133.9 (s, C_{Acr}),

131.8 (s, $C_{Ar}-H$), 129.7 (s, $C_{Acr}-H$), 129.4 (br, $C_{Ar}-H$), 129.1 (br, $C_{Ar}-H$), 128.9 (s, C_{Acr}), 127.2 (s, $C_{Acr}-H$), 79.0 (t, $^2J_{CP} = 6.3$ Hz, η^2,η^2 -COD: Ir ($CH = CH_2$)₂), 32.6 (d, $^1J_{CP} = 30.5$ Hz, $C_{Acr}-CH_2-P$), 32.0 (s, η^2,η^2 -COD: $CH(CH_2)_4CH$). $^{31}P\{^1H\}$ NMR (202 MHz, acetone- d_6): 11.9 (s). ESI-HRMS (MeOH): M^+ , m/z 876.2531; calcd. for $C_{47}H_{43}IrNP_2$ (complex - BF_4^-), 876.2500.

Declaration of Competing Interest

The authors declare that they have no known competing financial interests or personal relationships that could have appeared to influence the work reported in this paper.

Data availability

Data will be made available on request.

Acknowledgments

We dedicate this manuscript to Professor Howard Alper in recognition of his outstanding contributions to science. YL is grateful to the Feinberg Graduate School, Weizmann Institute of Science, for a PhD fellowship.

Appendix A. Supplementary data

Multinuclear NMR spectra, IR spectra, crystallographic information for all crystal structures, crystal structure of complex **8**, ICP-OES data. Supplementary data to this article can be found online at <https://doi.org/10.1016/j.ica.2023.121787>.

References

- [1] C. Gunanathan, D. Milstein, Selective Synthesis of Primary Amines Directly from Alcohols and Ammonia, *Angew. Chem. Int. Ed.* **47** (2008) 8661–8664, <https://doi.org/10.1002/anie.200803229>.
- [2] S. Kar, D. Milstein, Sustainable Catalysis with Fluxional Acridine-Based PNP Pincer Complexes, *Chem. Commun.* **58** (2022) 3731–3746, <https://doi.org/10.1039/DCCO0247G>.
- [3] C. Gunanathan, L.J.W. Shimon, D. Milstein, Direct Conversion of Alcohols to Acetals and H_2 Catalyzed by an Acridine-Based Ruthenium Pincer Complex, *J. Am. Chem. Soc.* **131** (2009) 3146–3147, <https://doi.org/10.1021/ja808893g>.
- [4] U. Gellrich, J.R. Khusnudinova, G.M. Leitus, D. Milstein, Mechanistic Investigations of the Catalytic Formation of Lactams from Amines and Water with Liberation of H_2 , *J. Am. Chem. Soc.* **137** (2015) 4851–4859, <https://doi.org/10.1021/jacs.5b01750>.
- [5] J. Luo, S. Kar, M. Rauch, M. Montag, Y. Ben-David, D. Milstein, Efficient Base-Free Aqueous Reforming of Methanol Homogeneously Catalyzed by Ruthenium Exhibiting a Remarkable Acceleration by Added Catalytic Thiol, *J. Am. Chem. Soc.* **143** (2021) 17284–17291, <https://doi.org/10.1021/jacs.1c09007>.
- [6] Q.-Q. Zhou, Y.-Q. Zou, Y. Ben-David, D. Milstein, A Reversible Liquid-to-Liquid Organic Hydrogen Carrier System Based on Ethylene Glycol and Ethanol, *Chem. Eur. J.* **26** (2020) 15487–15490, <https://doi.org/10.1002/chem.202002749>.
- [7] Y.-Q. Zou, N. von Wolff, A. Anaby, Y. Xie, D. Milstein, Ethylene Glycol as an Efficient and Reversible Liquid-Organic Hydrogen Carrier, *Nat. Catal.* **2** (2019) 415–422, <https://doi.org/10.1038/s41929-019-0265-z>.
- [8] S. Kar, J. Luo, M. Rauch, Y. Diskin-Posner, Y. Ben-David, D. Milstein, Dehydrogenative Ester Synthesis from Enol Ethers and Water with a Ruthenium Complex Catalyzing Two Reactions in Synergy, *Green Chem.* **24** (2022) 1481–1487, <https://doi.org/10.1039/DIGC04574A>.
- [9] S. Tang, M. Rauch, M. Montag, Y. Diskin-Posner, Y. Ben-David, D. Milstein, Catalytic Oxidative Deamination by Water with H_2 Liberation, *J. Am. Chem. Soc.* **142** (2020) 20875–20882, <https://doi.org/10.1021/jacs.0c10826>.
- [10] X. Ye, P.N. Plessow, M.K. Brinks, M. Schelwies, T. Schaub, F. Rominger, R. Paciello, M. Limbach, P. Hofmann, Alcohol Amination with Ammonia Catalyzed by an Acridine-Based Ruthenium Pincer Complex: A Mechanistic Study, *J. Am. Chem. Soc.* **136** (2014) 5923–5929, <https://doi.org/10.1021/ja409368a>.
- [11] D. Pinggen, J.B. Schwaderer, J. Walter, J. Wen, G. Murray, D. Vogt, S. Mecking, Diamines for Polymer Materials via Direct Amination of Lipid- and Lignocellulose-based Alcohols with NH_3 , *ChemCatChem* **10** (2018) 3027–3033, <https://doi.org/10.1002/cctc.201800365>.
- [12] D. Pinggen, J.H. Choi, H. Allen, G. Murray, P. Ganji, P.W.N.M. van Leeuwen, M.H. G. Precht, D. Vogt, Amide versus Amine Ligand Paradigm in the Direct Amination of Alcohols with Ru-PNP Complexes, *Catal. Sci. Technol.* **8** (2018) 3969–3976, <https://doi.org/10.1039/C8CY00869H>.
- [13] C. Gunanathan, B. Gnnaprakasam, M.A. Iron, L.J.W. Shimon, D. Milstein, “Long-Range” Metal-Ligand Cooperation in H_2 Activation and Ammonia-Promoted Hydride Transfer with a Ruthenium-Acidine Pincer Complex, *J. Am. Chem. Soc.* **132** (2010) 14763–14765, <https://doi.org/10.1021/ja107770y>.
- [14] Y. Xie, Y. Ben-David, L.J.W. Shimon, D. Milstein, Highly Efficient Process for Production of Biofuel from Ethanol Catalyzed by Ruthenium Pincer Complexes, *J. Am. Chem. Soc.* **138** (2016) 9077–9080, <https://doi.org/10.1021/jacs.6b05433>.
- [15] J.R. Khusnudinova, Y. Ben-David, D. Milstein, Oxidant-Free Conversion of Cyclic Amines to Lactams and H_2 Using Water As the Oxygen Atom Source, *J. Am. Chem. Soc.* **136** (2014) 2998–3001, <https://doi.org/10.1021/ja500026m>.
- [16] J.R. Khusnudinova, D. Milstein, Metal-Ligand Cooperation, *Angew. Chem. Int. Ed.* **54** (2015) 12236–12273, <https://doi.org/10.1002/anie.201503873>.
- [17] J. Luo, M. Rauch, L. Avram, Y. Ben-David, D. Milstein, Catalytic Hydrogenation of Thioesters, Thiocarbamates, and Thioamides, *J. Am. Chem. Soc.* **142** (2020) 21628–21633, <https://doi.org/10.1021/jacs.0c10884>.
- [18] S. Kar, M. Rauch, G. Leitus, Y. Ben-David, D. Milstein, Highly Efficient Additive-Free Dehydrogenation of Neat Formic Acid, *Nat. Catal.* **4** (2021) 193–201, <https://doi.org/10.1038/s41929-021-00575-4>.
- [19] J. Luo, M. Rauch, L. Avram, Y. Diskin-Posner, G. Shmul, Y. Ben-David, D. Milstein, Formation of Thioesters by Dehydrogenative Coupling of Thiols and Alcohols with H_2 Evolution, *Nat. Catal.* **3** (2020) 887–892, <https://doi.org/10.1038/s41929-020-00514-9>.
- [20] J. Luo, Y. Liang, M. Montag, Y. Diskin-Posner, L. Avram, D. Milstein, Controlled Selectivity through Reversible Inhibition of the Catalyst: Stereodivergent Semihydrogenation of Alkynes, *J. Am. Chem. Soc.* **144** (2022) 13266–13275, <https://doi.org/10.1021/jacs.2c04233>.
- [21] P. Daw, A. Kumar, D. Oren, N.A. Espinosa-Jalapa, D. Srimani, Y. Diskin-Posner, G. Leitus, L.J.W. Shimon, R. Carmieli, Y. Ben-David, D. Milstein, Redox Noninnocent Nature of Acridine-Based Pincer Complexes of 3d Metals and C-C Bond Formation, *Organometallics* **39** (2020) 279–285, <https://doi.org/10.1021/acs.organomet.9b00607>.
- [22] W. Zuo, Method for Preparing Bis(2-dimethylaminoethyl) Ether or N, N, N-Tetramethyl-1,6-hexamidine by Alcohol Amination Under Homogeneous Catalysis, *CN2018-11318561* (2019).
- [23] W. Li, J.H. Xie, H. Lin, Q.L. Zhou, Highly Efficient Hydrogenation of Biomass-Derived Levulinic Acid to γ -Valerolactone Catalyzed by Iridium Pincer Complexes, *Green Chem.* **14** (2012) 2388–2390, <https://doi.org/10.1039/c2gc35650c>.
- [24] D.H.M.W. Thewissen, H.P.M.M. Ambrosius, H.L.M. Van Gaal, J.J. Steggerda, The Chemistry of Hetero-Allene and -Allylic Derivatives with Rhodium and Iridium II, Rhodium(I), and Iridium(I)-Phosphine Complexes of Hetero-Allylic Ligands of the Type $[Ph_2PC(x)NR]^-$ ($X = S, NR, O$) and $[Ph_2PW(C(S)NR)^-$ ($Q = S, O$). Synthesis and ^{31}P -NMR, *J. Organomet. Chem.* **192** (1) (1980) 101–113.
- [25] G.R. Fulmer, A.J.M. Miller, N.H. Sherden, H.E. Gottlieb, A. Nudelman, B.M. Stoltz, J.E. Bercaw, K.I. Goldberg, NMR Chemical Shifts of Trace Impurities: Common Laboratory Solvents, Organics, and Gases in Deuterated Solvents Relevant to the Organometallic Chemist, *Organometallics* **29** (2010) 2176–2179, <https://doi.org/10.1021/om100106e>.
- [26] H.C. Böttcher, M. Graf, K. Karaghiosoff, P. Mayer, Towards Rhodium and Iridium Complexes Containing the Secondary Phosphane Ligand $'Bu_2PH$, *Z. Anorg. Allg. Chem.* **633** (2007) 2374–2379, <https://doi.org/10.1002/zaac.20070259>.
- [27] R.J. Restivo, G. Ferguson, T.L. Kelly, C.V. Senoff, Metal-Olefin Complexes: Synthesis and Molecular Structure of *trans*-Chloro(ethylene)bis(triphenylphosphine)iridium(0), $IrCl(C_2H_4)(PPh_3)_2$, *J. Organomet. Chem.* **90** (1975) 101–109, [https://doi.org/10.1016/S0022-328X\(00\)91614-4](https://doi.org/10.1016/S0022-328X(00)91614-4).
- [28] T. Ohmura, K. Yagi, T. Torigoe, M. Sugino, Intramolecular Addition of a Dimethylamino $C(sp^3)-H$ Bond across C–C Triple Bonds Using $IrCl(DTBM-SEGPHOS)$ (ethylene) Catalyst: Synthesis of Indoles from 2-Alkynyl-N-methylanilines, *Synthesis* **53** (2021) 3057–3064, <https://doi.org/10.1055/a-1511-1025>.
- [29] E. Hirota, Y. Endo, S. Saito, K. Yoshida, I. Yamaguchi, K. Machida, Microwave Spectra of Deuterated Ethylenes: Dipole Moment and r_g Structure, *J. Mol. Spectrosc.* **89** (1981) 223–231, [https://doi.org/10.1016/0022-2852\(81\)90171-5](https://doi.org/10.1016/0022-2852(81)90171-5).
- [30] D.E. Shaw, D.W. Lepard, H.L. Welsh, A_0 Value and Structural Parameters of the Ethane Molecule, *J. Chem. Phys.* **42** (1965) 3736–3737. 10.1063/1.1695799.
- [31] S. Alvarez, A Cartography of the van der Waals Territories, *Dalton Trans.* **42** (2013) 8617–8636, <https://doi.org/10.1039/c3dt50599e>.
- [32] P.B. Chock, J. Halpern, Kinetics of the Addition of Hydrogen, Oxygen, and Methyl Iodide to Some Square-Planar Iridium(I) Complexes, *J. Am. Chem. Soc.* **88** (1966) 3511–3514, <https://doi.org/10.1021/ja00967a009>.
- [33] A.L. Sargent, M.B. Hall, Theoretical Studies of Inorganic and Organometallic Reaction Mechanisms. 4. Oxidative Addition of Dihydrogen to d^8 Square-Planar Iridium Complexes with *trans* Phosphines, *Inorg. Chem.* **31** (1992) 317–321, <https://doi.org/10.1021/ic00028a036>.
- [34] M.J. Burk, M.P. McGrath, R. Wheeler, R.H. Crabtree, The Origin of the Directing Effect in Hydrogen Addition to Square-Planar d^8 Complexes, *J. Am. Chem. Soc.* **110** (1988) 5034–5039.
- [35] O. Blum, D. Milstein, Hydride Elimination from an Iridium(III) Alkoxide Complex: A Case in Which a Vacant *cis* Coordination Site is not Required, *J. Organomet. Chem.* **593**–594 (2000) 479–484, [https://doi.org/10.1016/S0022-328X\(99\)00619-1](https://doi.org/10.1016/S0022-328X(99)00619-1).
- [36] Z.E. Clarke, P.T. Maragh, T.P. Dasgupta, D.G. Gusev, A.J. Lough, K. Abdur-Rashid, A Family of Active Iridium Catalysts for Transfer Hydrogenation of Ketones, *Organometallics* **25** (2006) 4113–4117, <https://doi.org/10.1021/om060049z>.
- [37] Y. Pan, C. Guan, H. Li, P. Chakraborty, C. Zhou, K.-W. Huang, CO_2 Hydrogenation by Phosphorus-Nitrogen PN^3P -Pincer Iridium Hydride Complexes: Elucidation of

- the Deactivation Pathway, Dalton Trans. 48 (2019) 12812–12816, <https://doi.org/10.1039/C9DT01319A>.
- [38] J. Bi, P. Hou, P. Kang, Single Iridium Pincer Complex for Roundtrip Electrochemical Conversion between Carbon Dioxide and Formate, ChemCatChem 11 (2019) 2069–2072, <https://doi.org/10.1002/cctc.201900083>.
- [39] B.L. Haymore, J.D. Lamb, R.M. Izatt, J.J. Christensen, Thermodynamic Origin of the Macrocyclic Effect in Crown Ether Complexes of Na^+ , K^+ , and Ba^{2+} , Inorg. Chem. 21 (1982) 1598–1602, <https://doi.org/10.1021/ic00134a065>.
- [40] J.D. Lamb, R.M. Izatt, C.S. Swain, J.J. Christensen, A Systematic Study of the Effect of Macrocyclic Ring Size and Donor Atom Type on the $\log K$, ΔH , and ΔS of Reactions at 25 °C in Methanol of Mono- and Divalent Cations with Crown Ethers, J. Am. Chem. Soc. 102 (1980) 475–479, <https://doi.org/10.1021/ja00522a005>.
- [41] H. Saito, R. Tabeta, A High Resolution ^{23}Na NMR Study of Sodium Complexes with Ionophores in Solution. Stability of Complexes as Viewed from Displacements of ^{23}Na Chemical Shifts as Referred to Those in the Solid State, Bull. Chem. Soc. Jpn. 60 (1987) 61–68, <https://doi.org/10.1246/bcsj.60.61>.
- [42] L. Fan, S. Parkin, O.V. Ozarov, Halobenzenes and Ir(I): Kinetic C–H Oxidative Addition and Thermodynamic C–Hal Oxidative Addition, J. Am. Chem. Soc. 127 (2005) 16772–16773, <https://doi.org/10.1021/ja0557637>.
- [43] N. Grüger, H. Wadeppohl, L.H. Gade, Iridium Complexes Containing a PNP Pincer Ligand: Syntheses, Structural Chemistry, and Bond Activations, Eur. J. Inorg. Chem. 2013 (2013) 5358–5365, <https://doi.org/10.1002/ejic.201300857>.
- [44] C. Cheng, B.G. Kim, D. Guironnet, M. Brookhart, C. Guan, D.Y. Wang, K. Krogh-Jespersen, A.S. Goldman, Synthesis and Characterization of Carbazolide-Based Iridium PNP Pincer Complexes. Mechanistic and Computational Investigation of Alkene Hydrogenation: Evidence for an Ir(III)/Ir(V)/Ir(III) Catalytic Cycle, J. Am. Chem. Soc. 136 (2014) 6672–6683, <https://doi.org/10.1021/ja501572g>.
- [45] A.S. Goldman, J. Halpern, Reactivity Patterns and Catalytic Chemistry of Iridium Polyhydride Complexes, J. Organometal. Chem. 382 (1990) 237–253, [https://doi.org/10.1016/0022-328X\(90\)85230-V](https://doi.org/10.1016/0022-328X(90)85230-V).
- [46] D.W. Lee, W.C. Kaska, C.M. Jensen, Mechanistic Features of Iridium Pincer Complex Catalyzed Hydrocarbon Dehydrogenation Reactions: Inhibition upon Formation of a μ -Dinitrogen Complex, Organometallics 17 (1998) 1–3, <https://doi.org/10.1021/om970769>.
- [47] D.W. Lee, C.M. Jensen, D. Morales-Morales, Reactivity of Iridium PCP Pincer Complexes toward CO and CO_2 . Crystal Structures of $\text{IrH}(\kappa^2\text{-O}_2\text{COH})\{\text{C}_6\text{H}_3\text{-2,6-(CH}_2\text{PBu}_2)_2\}$ and $\text{IrH}(\text{C(OOH)}\{\text{C}_6\text{H}_3\text{-2,6-(CH}_2\text{PBu}_2)_2\}\text{-H}_2\text{O}$, Organometallics 22 (2003) 4744–4749, <https://doi.org/10.1021/om030453n>.
- [48] R. Ghosh, M. Kanzelberger, T.J. Emge, G.S. Hall, A.S. Goldman, Dinitrogen Complexes of Pincer-Ligated Iridium, Organometallics 25 (2006) 5668–5671, <https://doi.org/10.1021/om0607043>.
- [49] J.M. Goldberg, S.D.T. Cherry, L.M. Guard, W. Kaminsky, K.I. Goldberg, D. M. Heinekey, Hydrogen Addition to (pincer)Ir^I(CO) Complexes: The Importance of Steric and Electronic Factors, Organometallics 35 (2016) 3546–3556, <https://doi.org/10.1021/acs.organomet.6b00598>.
- [50] J. Jover, J. Cirera, Computational Assessment on the Tolman Cone Angles for P-Ligands, Dalton Trans. 48 (2019) 15036–15048, <https://doi.org/10.1039/C9DT02876E>.
- [51] S. Nakayama, S. Morisako, M. Yamashita, Synthesis and Application of Pyrrole-Based PNP–Ir Complexes to Catalytic Transfer Dehydrogenation of Cyclooctane, Organometallics 37 (2018) 1304–1313, [https://doi.org/10.1021/organomet.8b00072](https://doi.org/10.1021/10.1021/organomet.8b00072).
- [52] M. Bosch, K. Ilg, H. Werner, Cationic Five-Coordinate Bis(butadiene)iridium(I) Complexes from the Highly Labile *cis*-[Ir($\eta^2\text{-C}_8\text{H}_{14}$)₂(acetone)₂]⁺ Cation as the Precursor, Eur. J. Inorg. Chem. 2001 (2001) 3181–3185, [https://doi.org/10.1002/1099-0682\(200112\)2001:12<3181::AID-EJIC3181>3.0.CO;2-Y](https://doi.org/10.1002/1099-0682(200112)2001:12<3181::AID-EJIC3181>3.0.CO;2-Y).
- [53] M.V. Jiménez, J. Fernández-Tornos, J.J. Pérez-Torrente, F.J. Modrego, S. Winterle, C. Cunchillos, F.J. Lahoz, L.A. Oro, Iridium(I) Complexes with Hemilabile N-Heterocyclic Carbenes: Efficient and Versatile Transfer Hydrogenation Catalysts, Organometallics 30 (2011) 5493–5508, <https://doi.org/10.1021/om200747k>.
- [54] R.S. Tanke, R.H. Crabtree, Thermal and Photochemical Carbon–Hydrogen Bond Reactions of Alkenes in (Tris(pyrazolyl)borato)iridium(I) Complexes, Inorg. Chem. 28 (1989) 3444–3447, <https://doi.org/10.1021/ic00317a010>.
- [55] J.C. Peters, J.D. Feldman, T.D. Tilley, Silylene Extrusion from a Silane: Direct Conversion of Me_3SiH_2 to an Iridium Silylene Dihydride, J. Am. Chem. Soc. 121 (1999) 9871–9872, <https://doi.org/10.1021/ja992367d>.
- [56] P.H.M. Budzelaar, N.N.P. Moonen, R. de Gelder, J.M.M. Smits, A.W. Gal, Rhodium and Iridium β -Diimine Complexes – Olefin Hydrogenation Step by Step, Eur. J. Inorg. Chem. 2000 (2000) 753–769, [https://doi.org/10.1002/\(SICI\)1099-0682\(200004\)2000:4<753::AID-EJIC753>3.0.CO;2-V](https://doi.org/10.1002/(SICI)1099-0682(200004)2000:4<753::AID-EJIC753>3.0.CO;2-V).
- [57] D.A. Ortmann, O. Gevert, M. Laubender, H. Werner, Square-Planar Bis(triisopropylstibine)(olefin)iridium(I) Complexes and Their Rearrangement to (η^3 -Allyl)hydridoiridium(III) Isomers, Organometallics 20 (2001) 1776–1782, <https://doi.org/10.1021/om001078r>.
- [58] L. Turculet, J.D. Feldman, T.D. Tilley, Coordination Chemistry and Reactivity of New Zwitterionic Rhodium and Iridium Complexes Featuring the Tripodal Phosphine Ligand [PhB(CH₂PPr₂)₃]⁻: Activation of H–H, Si–H, and Ligand B–C Bonds, Organometallics 23 (10) (2004) 2488–2502.
- [59] H.A. Ho, T.S. Gray, B. Baird, A. Ellern, A.D. Sadow, Allylic C–H Bond Activation and Functionalization Mediated by Tris(oxazolinyl)borato Rhodium(I) and Iridium (I) Compounds, Dalton Trans. 40 (2011) 6500–6514, <https://doi.org/10.1039/c1dt0249d>.
- [60] S. Xu, K. Manna, A. Ellern, A.D. Sadow, Mixed N-Heterocyclic Carbene–Bis(oxazolinyl)borato Rhodium and Iridium Complexes in Photochemical and Thermal Oxidative Addition Reactions, Organometallics 33 (2014) 6840–6860, <https://doi.org/10.1021/om500891h>.
- [61] T.F. Vaughan, J.L. Spencer, Transition Metal Complexes of the Pyridylphosphine Ligand o-C₆H₄(CH₂PPV₂)₂, Dalton Trans. 45 (2016) 16826–16837, <https://doi.org/10.1039/C6DT02041K>.
- [62] M.A. Cinelli, G. Minghetti, F. Cocco, S. Stoccero, A. Zucca, M. Manassero, M. Arca, Synthesis and Properties of Gold Alkene Complexes. Crystal Structure of [Au(bipy)^{oxy}]²⁻($\eta^2\text{-CH}_2\text{CHPh}$)[PF₆] and DFT Calculations on the Model Cation [Au(bipy)($\eta^2\text{-CH}_2\text{CH}_2$)⁺], Dalton Trans. (2006) 5703–5716, <https://doi.org/10.1039/B610657A>.
- [63] K. Hagen, L. Hedberg, K. Hedberg, Molecular Structure and Conformation of *cis,cis*-1,5-cyclooctadiene, J. Phys. Chem. 86 (1982) 117–121, <https://doi.org/10.1021/j100390a024>.
- [64] J.L. Herde, J.C. Lambert, C.V. Senoff, M.A. Cushing, Cyclooctene and 1,5-Cyclooctadiene Complexes of Iridium(I), Inorg. Synth. 15 (2007) 18–20, <https://doi.org/10.1021/9780470132463.ch05>.
- [65] TopSpin v.3.6.2, Bruker BioSpin GmbH, Ettlingen, Germany.
- [66] C.R. Groom, I.J. Bruno, M.P. Lightfoot, S.C. Ward, The Cambridge Structural Database, Acta. Cryst. B 72 (2016) 171–179, <https://doi.org/10.1107/S2052520616003954>.
- [67] I.J. Bruno, J.C. Cole, P.R. Edgington, M. Kessler, C.F. Macrae, P. McCabe, J. Pearson, R. Taylor, New Software for Searching the Cambridge Structural Database and Visualizing Crystal Structures, Acta. Cryst. B 58 (2002) 389–397, <https://doi.org/10.1107/S0108768102003324>.
- [68] C.F. Macrae, I. Sovago, S.J. Cottrell, P.T.A. Galek, P. McCabe, E. Pidcock, M. Platings, G.P. Shields, J.S. Stevens, M. Towler, P.A. Wood, Mercury 4.0: From Visualization to Analysis, Design and Prediction, J. Appl. Cryst. 53 (2020) 226–235, <https://doi.org/10.1107/S1600576719014092>.